HEAT-TRANSFER AND PRESSURE INVESTIGATION OF A FIN-PLATE INTERFERENCE MODEL AT A MACH NUMBER OF 6

by Robert A. Jones

Langley Research Center
Langley Station, Hampton, Va.

NATIONAL AERONAUTICS AND SPACE ADMINISTRATION • WASHINGTON, D. C. • JULY 1964

HEAT-TRANSFER AND PRESSURE INVESTIGATION

OF A FIN-PLATE INTERFERENCE MODEL

AT A MACH NUMBER OF 6

By Robert A. Jones

Langley Research Center
Langley Station, Hampton, Va.

NATIONAL AERONAUTICS AND SPACE ADMINISTRATION

HEAT-TRANSFER AND PRESSURE INVESTIGATION

OF A FIN-PLATE INTERFERENCE MODEL

AT A MACH NUMBER OF 6

By Robert A. Jones

SUMMARY

A 60° swept cylindrical-leading-edge fin mounted on a sharp flat plate was investigated at a Mach number of 6 over a range of Reynolds numbers, based on free-stream conditions and fin leading-edge diameter, from 0.062×10^6 to 0.77×10^6. The plate was maintained at zero angle of attack and the yaw angle of the fin was varied from 0° to 30°. A relatively weak shock wave which originated at the leading edge of the plate impinged on the leading edge of the fin. Heat-transfer rates and pressures were measured on both the plate and the fin. The measured data on the fin and plate are compared with values calculated from laminar and turbulent theories for an infinitely long 60° swept cylinder and undisturbed plate.

The results indicate that the primary effect of shock impingement and other interference was to promote transition to turbulent flow on the fin leading edge. The corresponding effect on the heat-transfer rate resulted in a range of values from approximately one to three times the calculated laminar values, depending on Reynolds number. Calculated heat-transfer rates at the stagnation line of the fin, based on the assumption of a turbulent boundary layer, were in agreement with the maximum measured values. High heat-transfer rates were also measured on the plate at locations near the impingement of the fin shock wave. In this case, the high rates occurred at all free-stream Reynolds numbers and the maximum values were considerably above those calculated from turbulent flat-plate theory based on conditions corresponding to the measured local pressure.

INTRODUCTION

The problem of heat transfer to aerodynamic control surfaces of hypersonic vehicles is complicated by mutual interference effects. Examples of such phenomena are the impingement of the body shock wave on the control surface and the corner interference between control surfaces and body surfaces. The effects of such interference on the heat-transfer rate are difficult to predict analytically. In addition, there is a scarcity of experimental data, particularly data showing the effects of Reynolds number on these phenomena. Previous investigations (for example, ref. 1) have shown that the heat-transfer rate may be

increased considerably by this interference, but additional work appears necessary for a complete understanding of the problem.

The present investigation was undertaken to study the effects of mutual interference on heat transfer of a 60° swept cylindrical-leading-edge fin and a sharp flat plate. Tests were made at a Mach number of approximately 6 over a range of Reynolds numbers, based on free-stream conditions and fin leading-edge diameter, from 0.062×10^6 to 0.77×10^6. The plate was kept at zero angle of attack and the yaw angle of the fin was varied from 0° to 30°. Heat-transfer rates and surface pressures were measured on both the fin and the plate.

SYMBOLS

a,b,c,d	stations on plate
A,B,C,D	stations on fin
c_p	specific heat of wall
C_p	pressure coefficient
$C_{p,max}$	maximum pressure coefficient
h	local heat-transfer coefficient
$h_{no\ fin}$	local heat-transfer coefficient on plate without fin
$h_{\Lambda=0}$	theoretical heat-transfer coefficient at stagnation line of an infinite unswept cylinder
l	length of plate
M_∞	free-stream Mach number
N_{St}	Stanton number, based on free-stream conditions
$N_{St,p}$	Stanton number, based on conditions for measured pressure
p	local surface pressure
$p_{no\ fin}$	local surface pressure on plate without fin
p_{sl}	stagnation-line pressure
$p_{t,\infty}$	isentropic stagnation pressure
$p_{t,\sigma}$	stagnation pressures behind a normal shock at free-stream Mach number
p_∞	free-stream static pressure

q	heat-transfer rate
r	radius of fin leading edge
$R_{D,\infty}$	Reynolds number, based on free-stream conditions and fin leading-edge diameter
$R_{x,\infty}$	Reynolds number, based on free-stream conditions and distance from plate leading edge
s	surface distance from plane of symmetry of fin leading edge (fig. 2)
t	time
T_e	local static temperature at outer edge of boundary layer
T_t	stagnation temperature
T_r	recovery temperature
T_w	wall temperature
x	distance from leading edge of plate (fig. 2)
y	distance along stagnation line of fin measured from plate-fin junction
β	yaw angle of fin
γ	ratio of specific heat at constant pressure to specific heat at constant volume
δ	Newtonian flow-deflection angle of component of flow normal to fin leading edge
ϵ	angle between leading edge of fin and free-stream direction
η	acute angle between component of free stream normal to leading edge of fin and plane of fin (s/r location of stagnation line)
$\theta = s/r$	
$\theta_{eff} = |\theta - \eta|$	angular location from stagnation line
Λ_{eff}	effective sweep, $90^\circ - \epsilon$
ρ	density
τ	thickness of wall

MODELS

Three sets of models were used in this investigation: One set contained thermocouples, one set contained pressure orifices, and one set was a dummy (no instrumentation). Although care was taken to make the three sets of models alike, slight differences could have existed between the heat-transfer and pressure configurations because data for the fin were obtained by using an instrumented fin and a dummy plate whereas data for the plate were obtained by using an instrumented plate and a dummy fin.

A photograph of the heat-transfer model (60° swept cylindrical-leading-edge fin mounted on a sharp-leading-edge flat plate) is presented in figure 1, and a sketch showing dimensions and thermocouple and pressure-orifice locations is presented in figure 2. The heat-transfer models were constructed with a wall thickness of 0.030 inch. Thermocouples made of 0.010-inch-diameter iron-constantan wire were spot welded to the inner surface of the wall. The wall was supported by webs which were located midway between thermocouple stations. The pressure models were constructed with a thick wall containing orifices approximately 0.040 inch in diameter. All models were made from type 347 stainless steel.

TUNNEL, TESTING TECHNIQUE, AND DATA REDUCTION

The investigation was conducted in a Mach number 6 low-density hypersonic tunnel at the Langley Research Center. The stagnation pressures used were approximately 40, 160, and 640 lb/sq in. gage with stagnation temperatures ranging from 350° F to 500° F, depending on the pressure. A complete description of this tunnel, as well as a more complete description of the testing technique and data-recording and data-reduction methods, is given in reference 2.

Heat-transfer data were obtained by using a transient testing technique in which the tunnel was started and brought to the desired operating conditions and then the model was rapidly injected into the airstream by a pneumatic piston. It was estimated that the time required for steady flow to be established after the model first entered the airstream was about 0.05 second. The model remained in the airstream about 5 seconds; however, heat-transfer data were obtained during the period from 0.1 to 1.1 seconds after the model first entered the airstream. Because of the short testing time, the model wall was practically isothermal and conduction effects were estimated to be negligible.

Thermocouple outputs were recorded on magnetic tape by a high-speed analog-to-digital data recording system at a rate of 40 points per second. Heat-transfer coefficients were obtained by fitting a second-degree curve to the data by the method of least squares and computing the time derivative of temperature on a card-programed computer. The heat-transfer coefficient, neglecting conduction, is given by the equation

$$h = \frac{\rho c_p \tau \frac{dT_w}{dt}}{T_r - T_w}$$

(1)

where the temperature potential $T_r - T_w$ was taken to be the calculated recovery temperature minus the measured wall temperature. The recovery temperature on the fin was calculated by assuming a laminar recovery factor $(T_r - T_e)/(T_t - T_e)$ of 0.85 and isentropic expansion of the flow from conditions behind a shock wave swept parallel to the fin leading edge to the calculated local surface pressure. The method of calculating the local surface pressure is discussed subsequently in the section entitled "Results and Discussion." For the plate the recovery temperature was calculated by assuming a laminar recovery factor of 0.85 and undisturbed flat-plate flow at the free-stream Mach number.

Pressures were recorded by photographing a mercury manometer board. Pressure data were obtained only at a Reynolds number, based on free-stream conditions and fin leading-edge diameter, of 0.70×10^6 because long testing times and high pressure levels were required for the manometer to settle out. The height of the mercury was read to the nearest 0.03 inch.

RESULTS AND DISCUSSION

Flow Pattern

Schlieren photographs of the flow are presented in figure 3. These photographs show that the strength of the leading-edge shock wave for the plate without fin is different from that for the plate with fin. In the "plate no fin" photograph, a plate instrumented with pressure orifices was used; whereas, in the "plate with fin" photographs, a dummy plate was used. However, any difference in plate leading-edge thickness is believed to be too small to cause the difference in shock strength. A comparison of the leading-edge shock wave for the plate without fin with that for the plate with fin can be seen more clearly in the sketch of figure 4, which is a sketch of the schlieren photographs for the fin at zero yaw. The shock wave for the plate without the fin is shown by the dashed line. The difference in the initial angle of the two shock waves is approximately 7°. As the yaw angle of the fin is increased (see fig. 3), the shape of the plate leading-edge shock wave remains practically unchanged. The mechanism by which the strength of this shock was different for the plate with fin and the plate without fin is not understood; however, the results of this investigation are believed to be valid even though this mechanism cannot be explained. In order to investigate the cause of this phenomenon, some schlieren photographs were made for different alinements of the plate relative to the free stream. A 1/2° expansion of the flow over the plate was found to result in a change in the shock shape for the plate with or without the fin, although the change was more pronounced when the fin was present. A small difference in alinement of the plates may therefore have contributed to the difference in shock shapes.

At the intersection of the plate shock wave and the fin shock wave, a faint line, which is thought to be a vortex line, was evident in all the schlieren photographs. The plate shock wave, which is relatively weak compared to the fin shock wave, appears to pass undisturbed through the fin shock and to intersect the fin. This apparent phenomenon is due to the greater width of the plate shock

wave (approximately 7 inches) and is actually the undisturbed plate shock which lies outside the region of interaction with the fin. Also shown in figure 4 are the thermocouple and pressure orifice stations of the fin. The two shock waves intersect nearest station B.

<center>Pressure Distributions on Fin</center>

Pressure distributions on the fin are presented in figure 5 as the ratio $p/p_{t,\sigma}$ plotted as a function of s/r, where p is the local measured pressure, $p_{t,\sigma}$ is the stagnation pressure behind a normal shock at the free-stream Mach number, and s/r is the distance from the plane of symmetry of the fin leading edge. The theoretical curve shown in this figure was computed from modified Newtonian theory, which predicts the distribution over the leading edge and downstream as

$$\frac{c_p}{c_{p,max}} = \sin^2\delta \tag{2}$$

where δ is the Newtonian deflection angle of the component of flow normal to the swept leading edge. This equation can be rewritten as

$$\frac{p}{p_{sl}} = \cos^2\theta_{eff} + \frac{p_\infty}{p_{sl}} \sin^2\theta_{eff} \tag{3}$$

where θ_{eff} is the complement of the flow deflection angle in a plane normal to the leading edge and p_{sl} is the stagnation-line pressure of the cylindrical leading edge computed from perfect-gas theory as follows:

$$\frac{p_{sl}}{p_{t,\infty}} = \left(\frac{2\gamma}{\gamma+1} M_\infty^2 \cos^2\Lambda_{eff} - \frac{\gamma-1}{\gamma+1}\right)^{\frac{-1}{\gamma-1}} \left(\frac{\frac{\gamma+1}{2} M_\infty^2 \cos^2\Lambda_{eff}}{1 + \frac{\gamma-1}{2} M_\infty^2}\right)^{\frac{\gamma}{\gamma-1}} \tag{4}$$

A comparison of pressure distributions computed by this method with experimental data for a 70° swept cylindrical-leading-edge slab at a Mach number of 6 is given in reference 3 and indicates good agreement for fin leading edges with no shock-wave impingement. The pressure distribution computed by equations (3) and (4) was used for determining the recovery temperature T_r of the fin (eq. (1)).

Figure 5 shows experimental pressures as much as 30 percent higher than theoretical pressures at station B (the station nearest the intersection of the shock waves for $\beta = 0°$) and also shows pressures somewhat higher than those predicted by theory at stations A and C. The fact that the pressures at stations D and E are in agreement with the theoretical curve indicates that the flow was similar to that of an infinitely long swept cylinder at those stations. For $\beta \geqq 15°$, the peak pressures at station C are greater than at station B, but the stagnation line is near $\theta = 30°$ ($s/r \approx 0.5$) and the shock impingement

6

might be closer to station C. As the angle of yaw increases, the pressure at station A for $\theta = 90^{\circ}$ (s/r = 1.56) becomes considerably lower than that predicated by theory and lower than the pressure at the other stations for $\theta = 90^{\circ}$. This indicates separation on the fin near the fin-plate juncture. The orifice of station A for $\theta = 90^{\circ}$ was very near this fin-plate juncture.

<center>Heat-Transfer Distribution on Fin</center>

The heat-transfer data on the fin are presented in figures 6, 7, and 8 as the ratio $h/h_{\Lambda=0}$, where h is the local experimental value of the heat-transfer coefficient based on a laminar recovery factor and $h_{\Lambda=0}$ is the theoretical laminar heat-transfer coefficient for the stagnation line of an unswept circular cylinder at free-stream conditions. The coefficient $h_{\Lambda=0}$ was computed by the method of reference 4. The curves shown in figure 6 represent a theoretical laminar heat-transfer-coefficient distribution which was computed from the following equation:

$$\frac{h}{h_{\Lambda=0}} = \frac{(h)_{\Lambda_{eff}}}{h_{\Lambda=0}} \frac{q}{(q)_{\theta_{eff}=0}} \frac{(T_r - T_w)_{\theta_{eff}=0}}{T_r - T_w} \tag{5}$$

where the ratio $\dfrac{(h)_{\Lambda_{eff}}}{h_{\Lambda=0}}$ was obtained from reference 4 and the ratio $\dfrac{q}{(q)_{\theta_{eff}=0}}$ was obtained by the method of reference 5 by using the theoretical pressure distribution from equations (3) and (4).

Previous investigations in this same facility have indicated that the flow over a fin leading edge with no interference would be laminar for the Reynolds numbers of this investigation. Reference 3 shows that for laminar flow, both the level and distribution of heat transfer to the leading edge of a swept fin could be reasonably predicted by the method used herein. Therefore, the high heat-transfer-coefficient ratios of figure 6 for the leading edge are apparently a result of the plate shock-wave impingement on the fin and the increased interference between the fin and the plate.

Similar large increases in heat transfer due to shock-wave impingement have been observed by other investigators; for example, reference 1 presents measured heating rates along an unswept circular cylinder at a Mach number of 4.44 and a Reynolds number, based on free-stream conditions and cylinder diameter, of 1.05×10^6. The measured values in the region of shock-wave impingement were approximately three times the calculated laminar values at the stagnation line. Since this cylinder was unswept, it is reasonable to expect that the flow at the stagnation line would have been laminar in the absence of shock-wave impingement.

In reference 6 are presented some heat-transfer results on a 60° swept cylinder protruding from an 8° wedge at a Mach number of 4.15. The measurements indicated that the flow over the cylinder, including the stagnation point, was turbulent, and the data were in agreement with calculated turbulent values in

the region of shock impingement. No effect of the shock impingement was detected in either the stagnation-line pressure or heat-transfer measurements.

In view of the different effects of shock-wave impingement on heat transfer, depending on whether the basic undisturbed flow was laminar or turbulent, which were reported in the previously mentioned experimental investigations (refs. 6 and 7), it is interesting to notice the effect on heat transfer of varying the Reynolds number in the present investigation. The increases in the heat-transfer coefficients of the fin leading edge which are due to the shock-wave impingement and plate interference varied from approximately one to three times the calculated laminar values, depending on Reynolds number. The increase was largest at the highest Reynolds number. For comparison, the heat-transfer coefficients of the stagnation line calculated by the method of reference 4 for turbulent flow are shown by the ticks on the ordinate of figure 6(a). The three values of $h/h_{\Lambda=0}$ of 0.497, 0.742, and 1.105 correspond to values of $R_{D,\infty}$ of 0.062×10^6, 0.21×10^6, and 0.77×10^6, respectively. At the lowest Reynolds number there was very little difference between the calculated laminar and turbulent values; however, at the highest Reynolds number this difference is large. The data for the highest Reynolds numbers are higher than the calculated turbulent values but these calculations were based on the calculated pressure of equation (4) rather than the measured pressure. If the measured pressure were used, the resulting value for the highest Reynolds number would be about 1.35 instead of the indicated value of 1.105. The agreement between the measured coefficients and the calculated turbulent values indicates that the primary effect of the shock impingement and fin-plate interference was to promote transition to turbulent flow. Since reference 6 found no effect for a shock impinging on a turbulent boundary layer, the calculated turbulent heat-transfer coefficients might serve as an upper limit for the effect of such interference. Additional experimental data for various shock strengths and Mach numbers, as well as for laminar and turbulent boundary layers, over a wide range of Reynolds numbers are necessary for a complete understanding of this phenomenon.

A cross plot of the data of figures 6(a) and 6(f) for the stagnation line $(\theta_{eff} = 0^\circ)$ is given in figures 7(a) and 7(b). The data of figures 7(a) and 7(b) are the faired values taken from figures 6(a) and 6(f), respectively. The trends for both 0° and 25° yaw are similar. The data of station A (y = 1 inch) appear to be strongly influenced by separation and other interference resulting from the fin-plate juncture. The data for y = 1 inch, $\beta = 25^\circ$ of figure 7(b) show larger heat-transfer coefficients than do the data for y = 1 inch, $\beta = 0^\circ$ of figure 7(a); this result is believed to be due to the increased interference from the fin-plate juncture at the higher yaw angle. Since the data for the lower Reynolds numbers are approximately equal and tend to approach the calculated laminar value as distance along the leading edge is increased, little effect of either shock-wave impingement or fin-plate interference is indicated. However, the data for the highest Reynolds number have a peak near the shock-wave impingement point with values for both yaw angles approximately equal to those calculated by assuming a turbulent boundary layer and measured pressures. In addition, at y = 5 inches, the values for the highest Reynolds number are still much larger than values calculated from the laminar theory.

8

An increase in the angle of yaw causes a shift in the s/r position of the stagnation line and a small increase in the calculated value $h/h_{\Lambda=0}$ at the stagnation line. There was a corresponding small increase in the measured values near the stagnation line, but otherwise the data of the leading edge at angle of yaw show the same trend as they did at zero yaw. Also, with an increase in the yaw angle, the heat-transfer coefficients for the slab portion of the fin ($s/r > 1.56$, fig. 6) increase considerably above those determined by theory and the highest values occur at the highest Reynolds numbers. The data of reference 3, for which there was no shock-wave impingement on the fin leading edge, show these same general trends. The high heating rates on the slab are therefore probably due to a combination of the fin-shock impingement on the plate and the corner interference between the fin and plate rather than to the shock impingement on the fin leading edge.

The fin was also tested at negative angles of yaw so that the instrumented portion of the fin was in the expansion region on the leeward side. The data for values of β from $-5°$ to $-15°$ are shown in figure 8. The data near $s/r = 0$ overlap the data of figure 6 and show the same results as already discussed; however, the data for large values of s/r are, of course, lower than on the windward side and show little or no variation with Reynolds number.

Pressure and Heat-Transfer Distribution on Plate

The pressures on the plate without the fin are presented in figure 9. The scatter of the data is within the accuracy of the measurements. The data agree with the calculated free-stream pressure based on the Mach number calibration of the tunnel.

Figure 10 shows the heat-transfer distribution on the plate without the fin and a theoretical laminar value calculated by the reference temperature method of reference 7. A large increase in heat-transfer rate occurs at the highest Reynolds number and it begins at $x/l \approx 0.6$, probably due to transition to turbulent flow. The transition Reynolds number, based on free-stream conditions and plate length, is about 5×10^6.

The pressure and heat-transfer data for the plate with the fin are presented in figure 11 as the ratio of the measured values with the fin to the measured values without the fin (figs. 9 and 10). Since this ratio is based on the measured data without the fin rather than on a calculated laminar value, the increased heat transfer due to transition shown in figure 10 for $R_{D,\infty} = 0.77 \times 10^6$ and $x/l > 0.5$ has the effect of an apparent reduction in the ratio $h/h_{no\ fin}$ for the high Reynolds number data of figure 11 for $x/l > 0.5$. For an example, see figure 11(g) at $x/l = 0.7$. Here, at station B, the ratio for $R_{D,\infty} = 0.77 \times 10^6$ is lower than the ratio for $R_{D,\infty} = 0.21 \times 10^6$; however, if the data for both Reynolds numbers had been based on a theoretical laminar value, the ratio for the high Reynolds number data would have been higher.

The effect of the fin-plate interference, indicated by figure 11, was to decrease the pressure ratio at some locations and to increase it in other locations. There was a decrease in pressure ratio ahead of the fin ($x/l < 0.3$) at

all angles of yaw. It was suggested previously that the increase in the leading-edge shock strength for the plate with the fin (fig. 4) might have been caused by a small error in alinement of the plate. A small expansion of the flow over the plate might cause a separation bubble at the leading edge of the plate followed by an expansion which caused the shock curvature. If this premise is correct, the low pressure ratios for $x/l < 0.3$ might be due to such an expansion. The largest pressure ratios usually occurred for locations between the fin and the impingement of the fin shock wave. When the fin was yawed, however, there were no two orifices located the same with respect to the fin-plate juncture.

Photographs showing the fin shock-wave impingement on a plate for a 70° swept fin are presented in figure 12. These photographs were made by placing the fin on a front-surfaced mirror and using a two-pass schlieren system. It was extremely difficult to get photographs of good quality because of strains in the mirror. The photographs shown were obtained as a part of an investigation for a 70° swept cylindrical-leading-edge fin; however, since a 10° difference in sweep angle should not significantly alter the pattern of shock impingement on the plate, figure 12 could be used to estimate the shock-impingement location for the present investigation.

Large heat-transfer-coefficient ratios for the plate are shown in figure 11. Comparisons with measurements taken from figure 12 indicate that the larger ratios occurred at locations near the fin shock-wave impingement. The general trend of higher heat-transfer-coefficient ratios at the higher Reynolds numbers indicates that the shock-wave impingement may promote transition to turbulent flow; however, separation and corner interference effects also influence the data and the effects of these different factors are difficult to identify. A plot of Stanton number as a function of Reynolds number (fig. 13) shows more clearly where the increase above laminar theory occurs.

Figure 13(a) presents data for the plate with the fin at zero yaw and compares these data with the results calculated from laminar and turbulent theories by the reference temperature method (ref. 7). The Stanton number of figure 13(a) is based on free-stream conditions. The marked increase above laminar theory occurs at three distinct values of $R_{x,\infty}$ and depends on the value of $R_{D,\infty}$. Measurements taken from figure 12 indicate that the shock-impingement location is at about $x/l = 0.5$ for station b. The values of $R_{x,\infty}$ corresponding to $x/l = 0.5$ are approximately 0.31×10^6, 1.05×10^6, and 3.85×10^6 for values of $R_{D,\infty}$ of 0.062×10^6, 0.21×10^6, and 0.77×10^6, respectively. The Reynolds numbers corresponding to the marked increase above laminar theory for station b shown in figure 13(a) are found to agree with the shock-impingement Reynolds numbers determined from figure 12. The fact that the increase begins at the point of shock-wave impingement, regardless of free-stream Reynolds number, is an indication that it was primarily the shock impingement which caused the increase since separation and other interference effects would probably occur at different x/l locations and different free-stream Reynolds numbers. However, investigations in which shock-wave impingement effects can be studied without the other interference effects which occurred in this study are necessary for a complete understanding of these phenomena. The data of figure 13(a) also indicate that these high heat-transfer rates were in some cases considerably

above calculated turbulent values and that these high rates occurred at all free-stream Reynolds numbers.

As the angle of yaw of the fin was increased, the maximum pressure ratios for the plate increased (fig. 11). Therefore, it was thought that Stanton numbers for a correlation of the type shown in figure 13 should be based on conditions corresponding to the measured local pressure. Such a correlation is shown in figure 13(b) for a yaw angle of 25°. In this plot the Stanton numbers $N_{St,p}$ were computed for conditions obtained by assuming that the free-stream flow was isentropically compressed to the measured local pressures for $R_{D,\infty} = 0.70 \times 10^6$ shown in figure 11(f). The trends shown are similar to those of figure 13(a) with the exception of the three very high heating rates shown by the circles that correspond to a location extremely near the fin-plate juncture at $x/l = 0.5$ (fig. 11(f)). These data may possibly have been influenced by conduction from the fin.

<center>SUMMARY OF RESULTS</center>

An experimental investigation of heat transfer and pressure in the interference region of a 60° swept cylindrical-leading-edge fin mounted on a sharp flat plate at a Mach number of 6 over a range of Reynolds numbers, based on free-stream conditions and fin leading-edge diameter, from 0.062×10^6 to 0.77×10^6 indicated the following results:

1. The shock-wave impingement on the leading edge of the fin, as well as other fin-plate interference effects, caused increases in heat transfer to the leading edge of the fin of approximately one to three times the calculated laminar values, depending on Reynolds number. The increase was largest at the highest Reynolds number.

2. Comparisons of the data with values calculated by assuming a turbulent boundary layer indicated that the primary effect of the shock-wave impingement, as well as other interference effects, was to promote transition to turbulent flow and that calculated values based on the assumption of turbulent flow might be used as an upper limit for estimating the heat-transfer rates to the fin leading edge.

3. Pressures and heat-transfer coefficients higher than flat-plate theoretical values were measured on the plate. The highest heat-transfer rates appeared to be for locations near the impingement of the fin shock wave. These high heat-transfer rates occurred at all free-stream Reynolds numbers and the maximum values were considerably above those calculated from turbulent flat-plate theory based on conditions corresponding to the measured local pressure.

Langley Research Center,
    National Aeronautics and Space Administration,
        Langley Station, Hampton, Va., March 5, 1964.

REFERENCES

1. Newlander, Robert A.: Effect of Shock Impingement on the Distribution of Heat-Transfer Coefficients on a Right Circular Cylinder at Mach Numbers of 2.65, 3.51, and 4.44. NASA TN D-642, 1961.

2. Jones, Robert A., and Gallagher, James J.: Heat-Transfer and Pressure Distributions of a 60° Swept Delta Wing With Dihedral at a Mach Number of 6 and Angles of Attack From 0° to 52°. NASA TM X-544, 1961.

3. Jones, Robert A., and Trimpi, Robert L.: Heat-Transfer and Pressure Distributions at a Mach Number of 6 for 70° Swept Slab Wings With Sharp and Spherical Noses and Cylindrical Leading Edges. NASA TM X-682, 1962.

4. Beckwith, Ivan E.: Similar Solutions for the Compressible Boundary Layer on a Yawed Cylinder With Transpiration Cooling. NASA TR R-42, 1959. (Supersedes NACA TN 4345.)

5. Lees, Lester: Laminar Heat Transfer Over Blunt-Nosed Bodies at Hypersonic Flight Speeds. Jet Propulsion, vol. 26, no. 4, Apr. 1956, pp. 259-269, 274.

6. Beckwith, Ivan E.: Experimental Investigation of Heat Transfer and Pressures on a Swept Cylinder in the Vicinity of Its Intersection With a Wedge and Flat Plate at Mach Number 4.15 and High Reynolds Numbers. NASA TN D-2020, 1964.

7. Eckert, Ernst R. G.: Survey on Heat Transfer at High Speeds. WADC Tech. Rep. 54-70, U.S. Air Force, Apr. 1954.
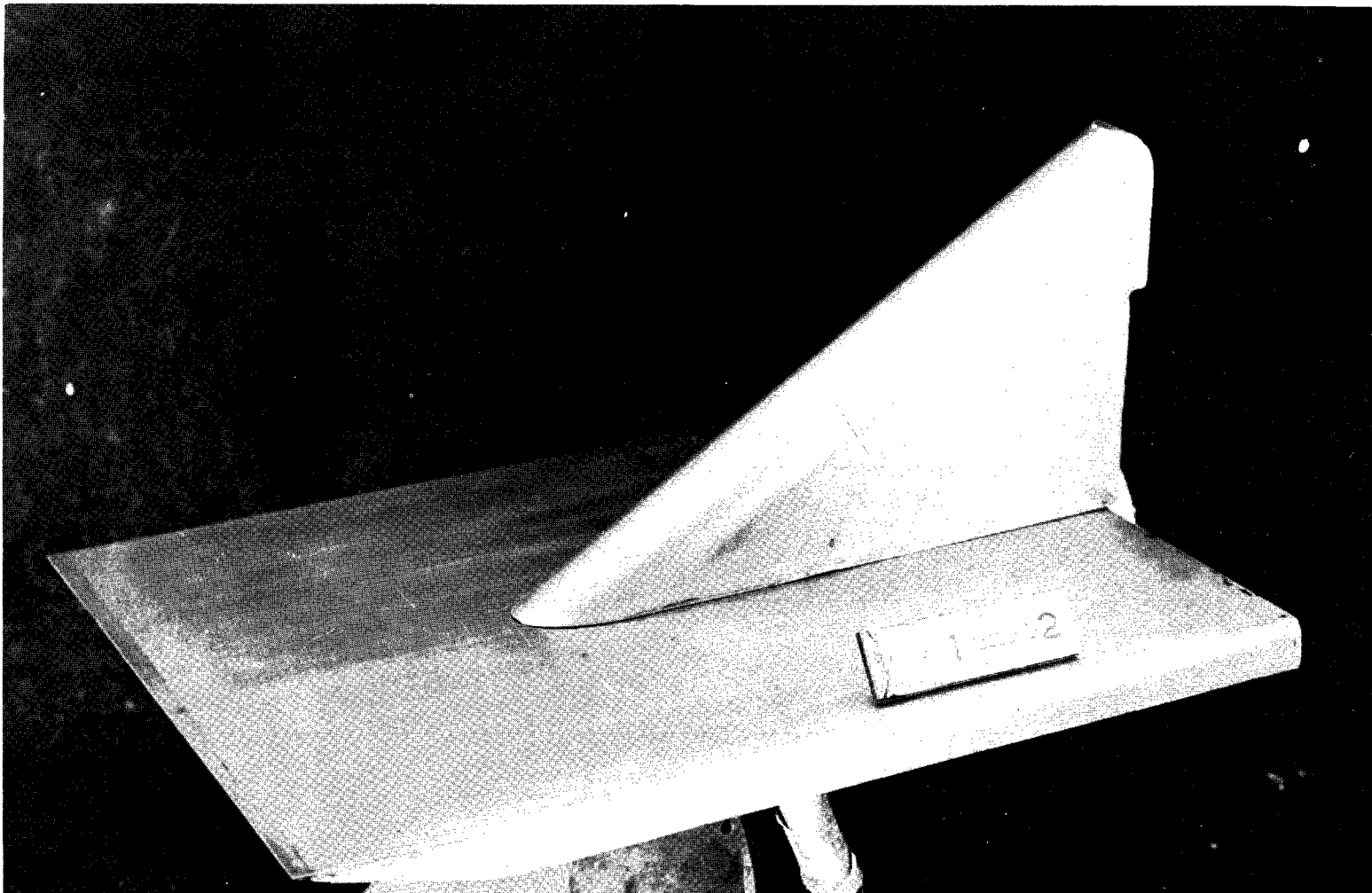
Figure 1.- Photograph of model.   L-61-8391

13

THERMOCOUPLE AND PRESSURE ORIFICE LOCATIONS

○ Indicates thermocouple
● Indicates pressure orifice

Plate				Fin		
x/l	Instrumentation		Stations	s/r	Instrumentation		Stations
0.1		●	a	-0.262	○	●	A,B,C,D,E
.2	○		a	0	○	●	A,B,C,D,E
.3	○	●	a,b	.262	○	●	A,B,C,D,E
.4	○	●	a,b,c,e	.524	○	●	A,B,C,D,E
.5	○	●	a,b,c,e	.785	○	●	A,B,C,D,E
.6	○	●	a,b,c,e	1.048	○		A,B,C,D,E
.7	○	●	a,b,c,d,e	1.309	○		A,B,C,D,E
.8	○	●	a,b,c,d,e	1.570	○	●	A,B,C,D,E
				1.968	○		B,C,D,E
				2.76	○		B,C,D,E
				3.40	○	●	D,E
				4.45	○		D
				5.34	○		E
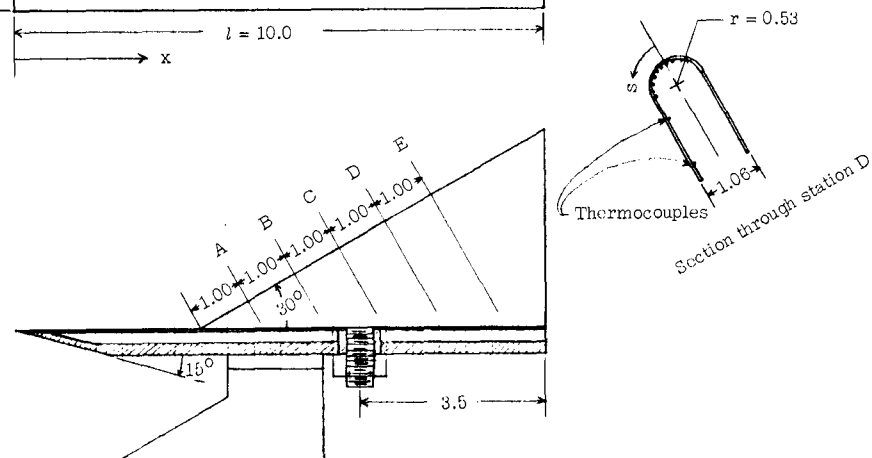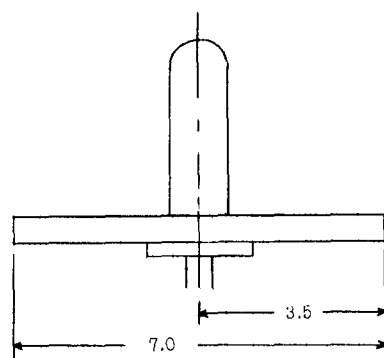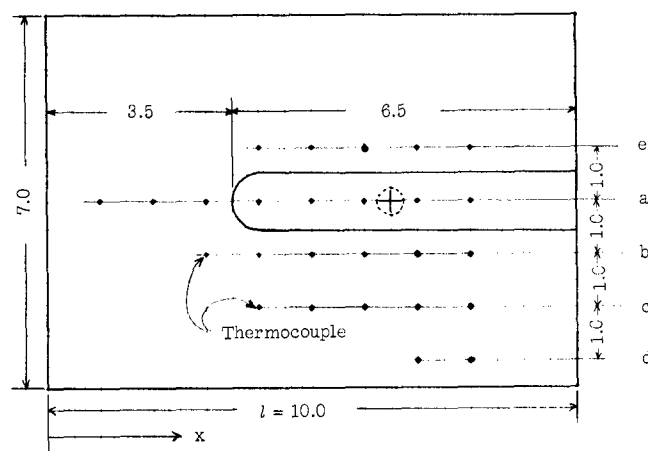
Figure 2.- Sketch of model. (All dimensions are in inches.)
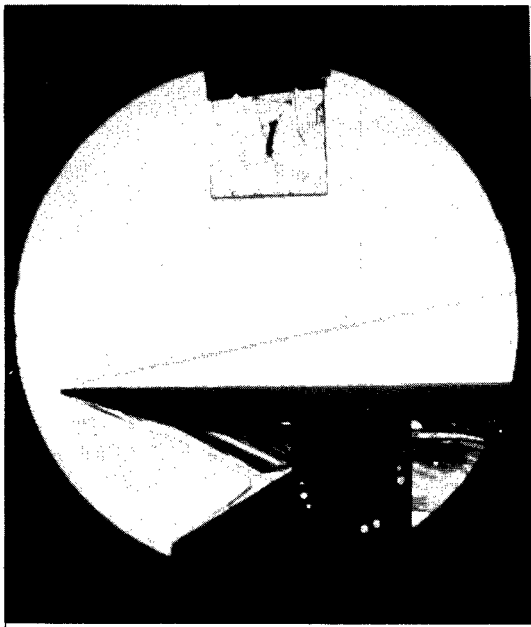
No fin
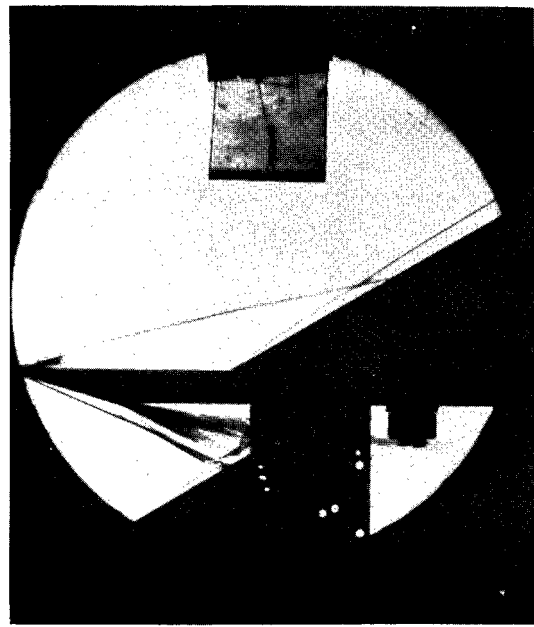
$\beta = 0^{\circ}$
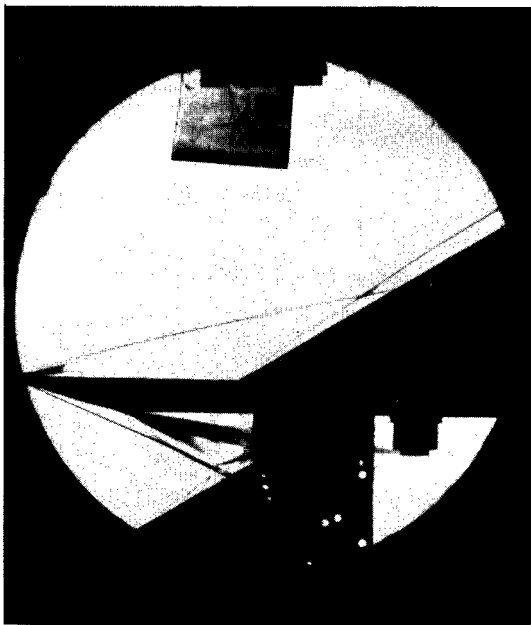
$\beta = 15^{\circ}$
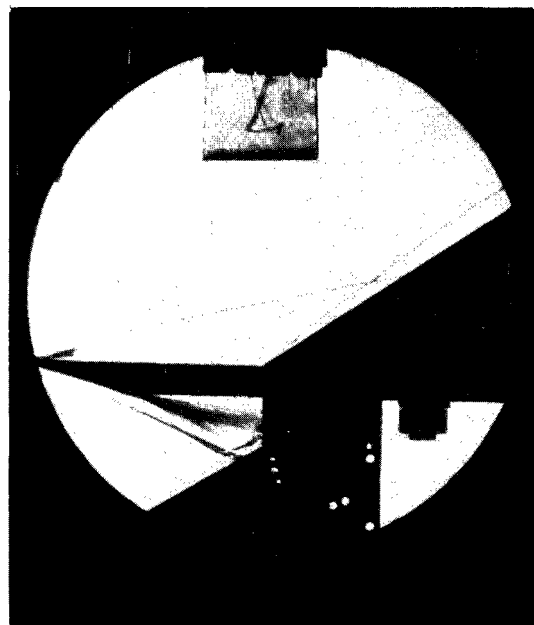
$\beta = 30^{\circ}$

Figure 3.- Schlieren photographs. $R_{D,\infty} = 0.70 \times 10^6$.

L-64-430

15

Fin shock wave

Shock wave for
plate without fin

Vortex line

E

D

Plate shock wave

C

B

A

10° 17°

Separation
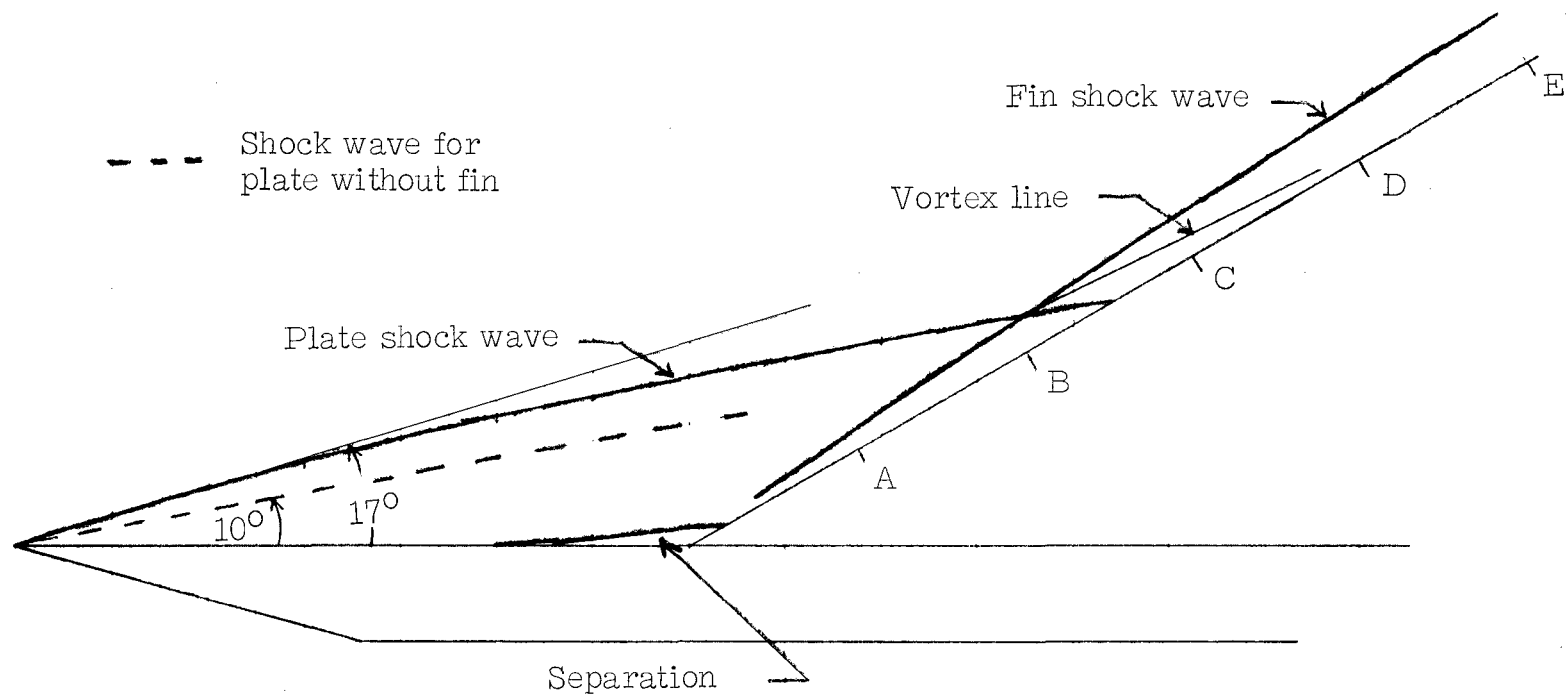
Figure 4.- Sketch of schlieren photograph. $\beta = 0^O$.
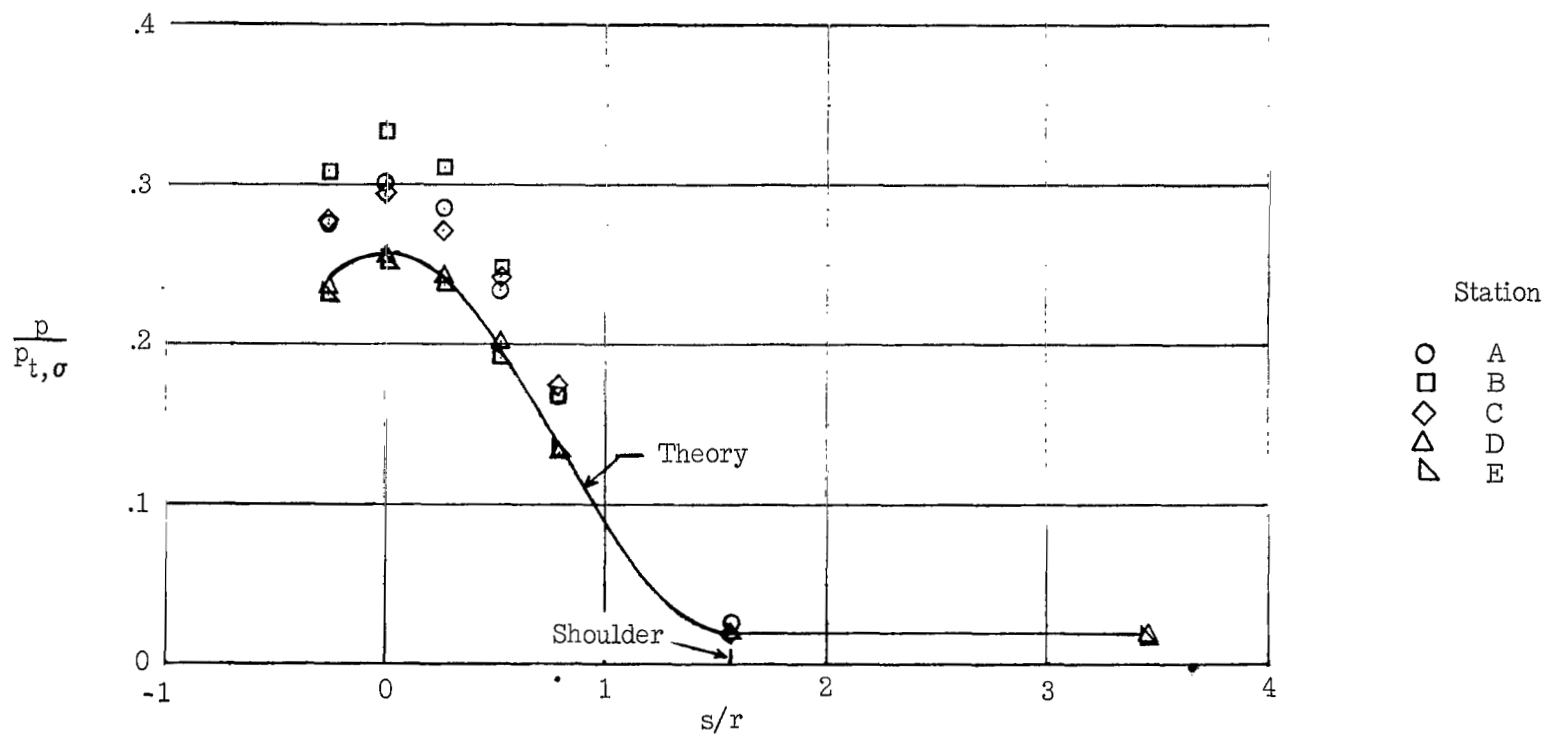
(a) $\beta = 0^\circ$.

Figure 5.- Pressure distribution on fin. $R_{D,\infty} = 0.70 \times 10^6$.
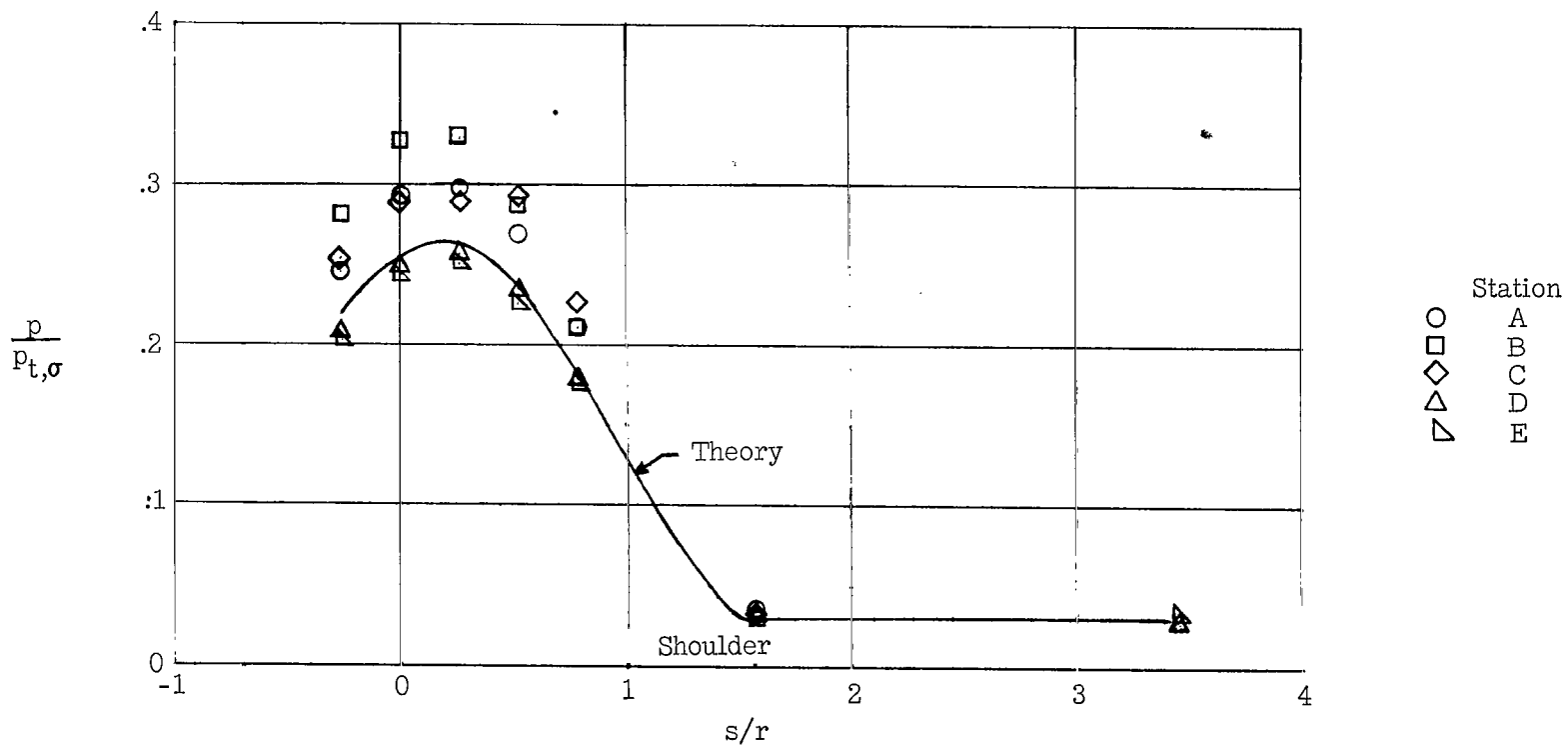
(b) $\beta = 5°$.

Figure 5.- Continued.
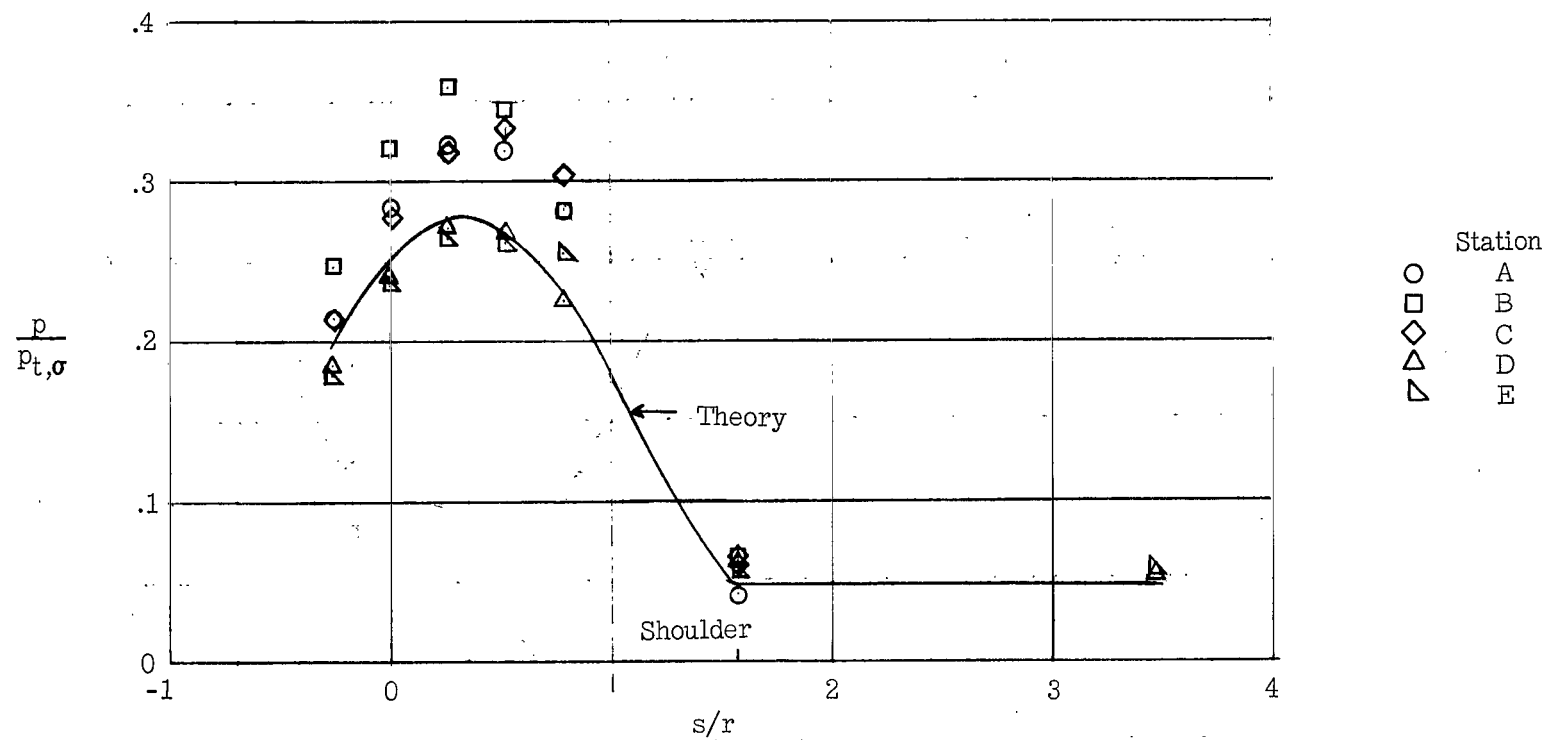
(c) $\beta = 10^{\circ}$.

Figure 5.- Continued.

(d) $\beta = 15^{o}$.
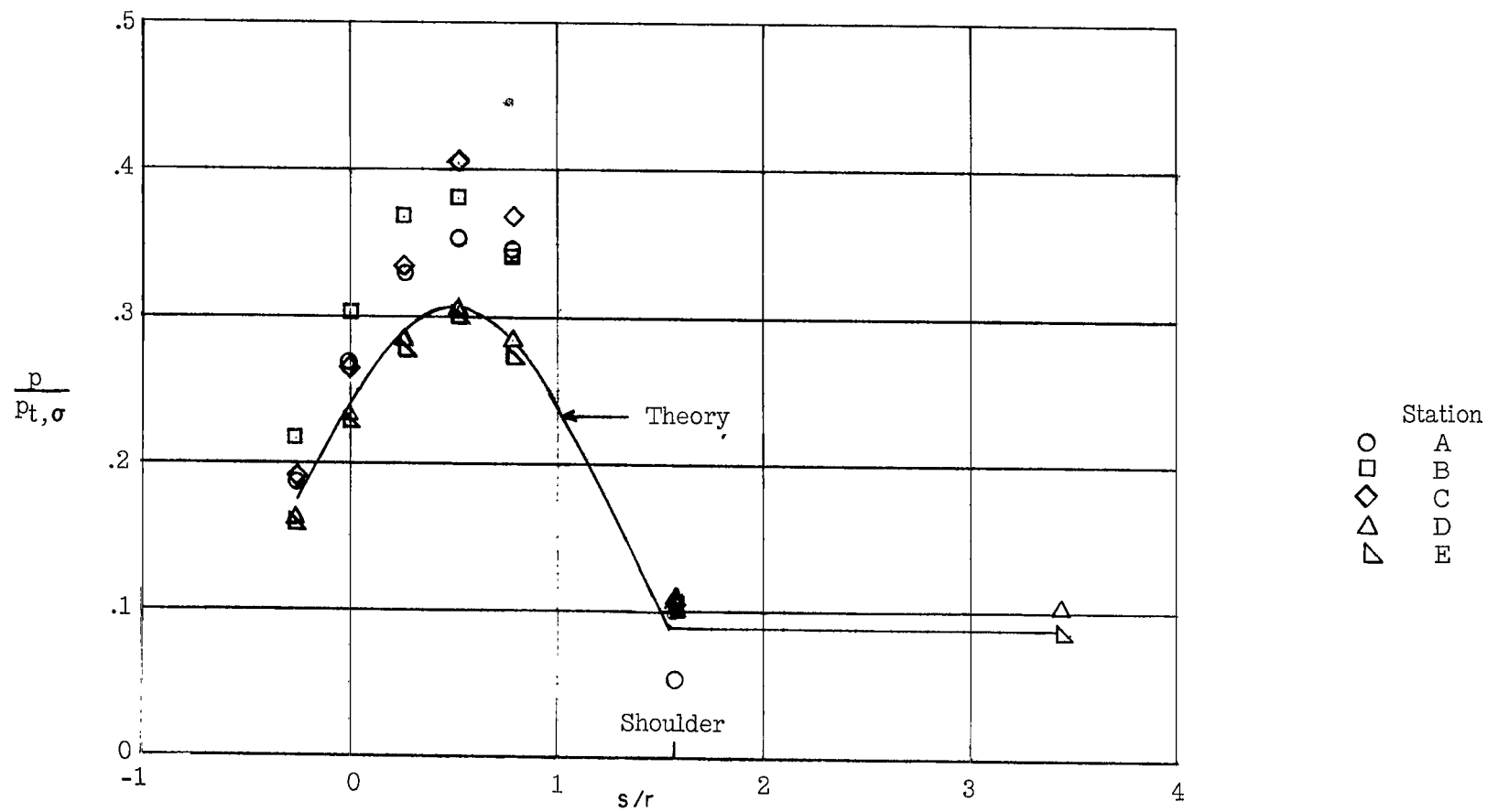
Figure 5.- Continued.

(e) $\beta = 20^{o}$.
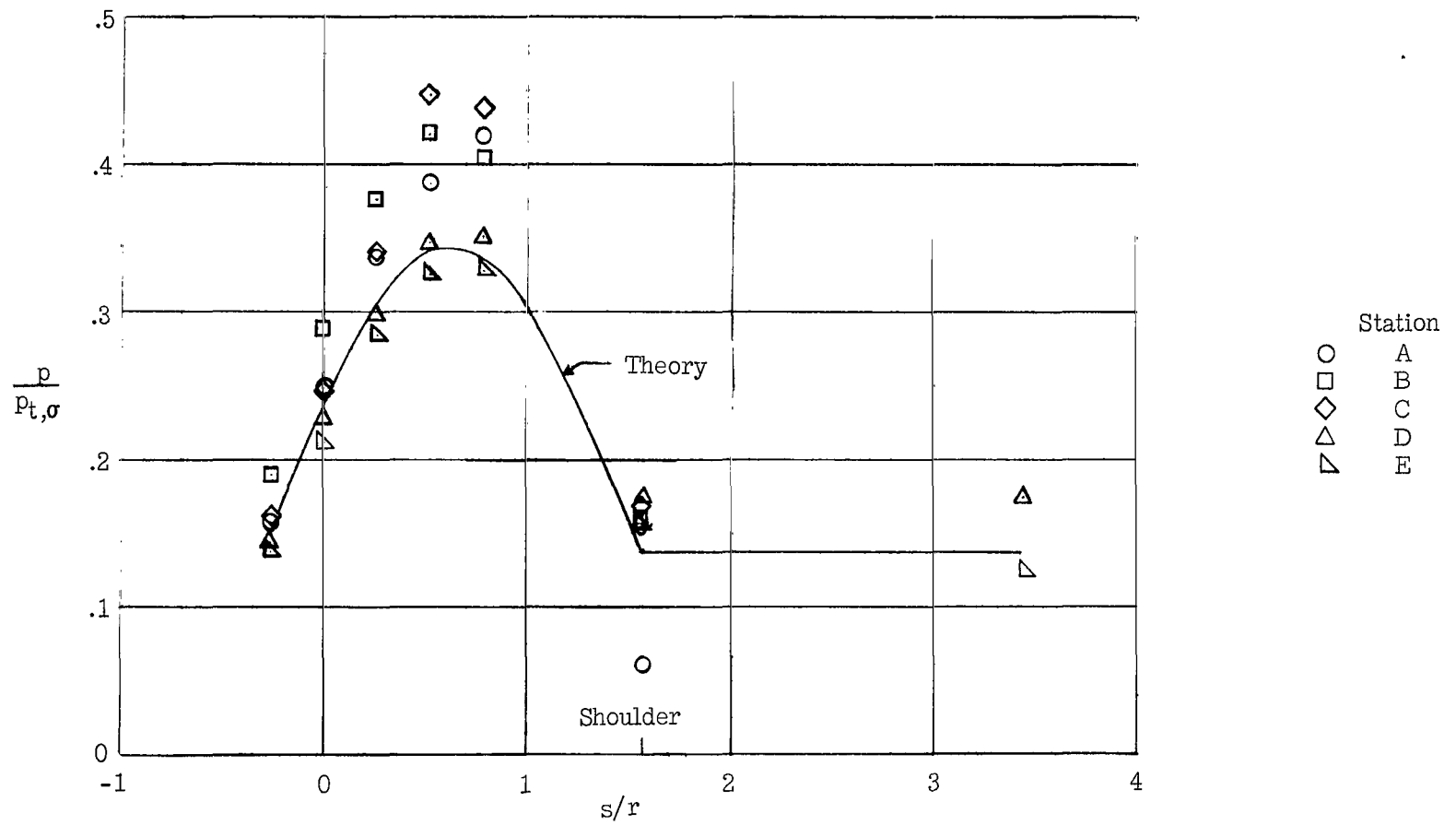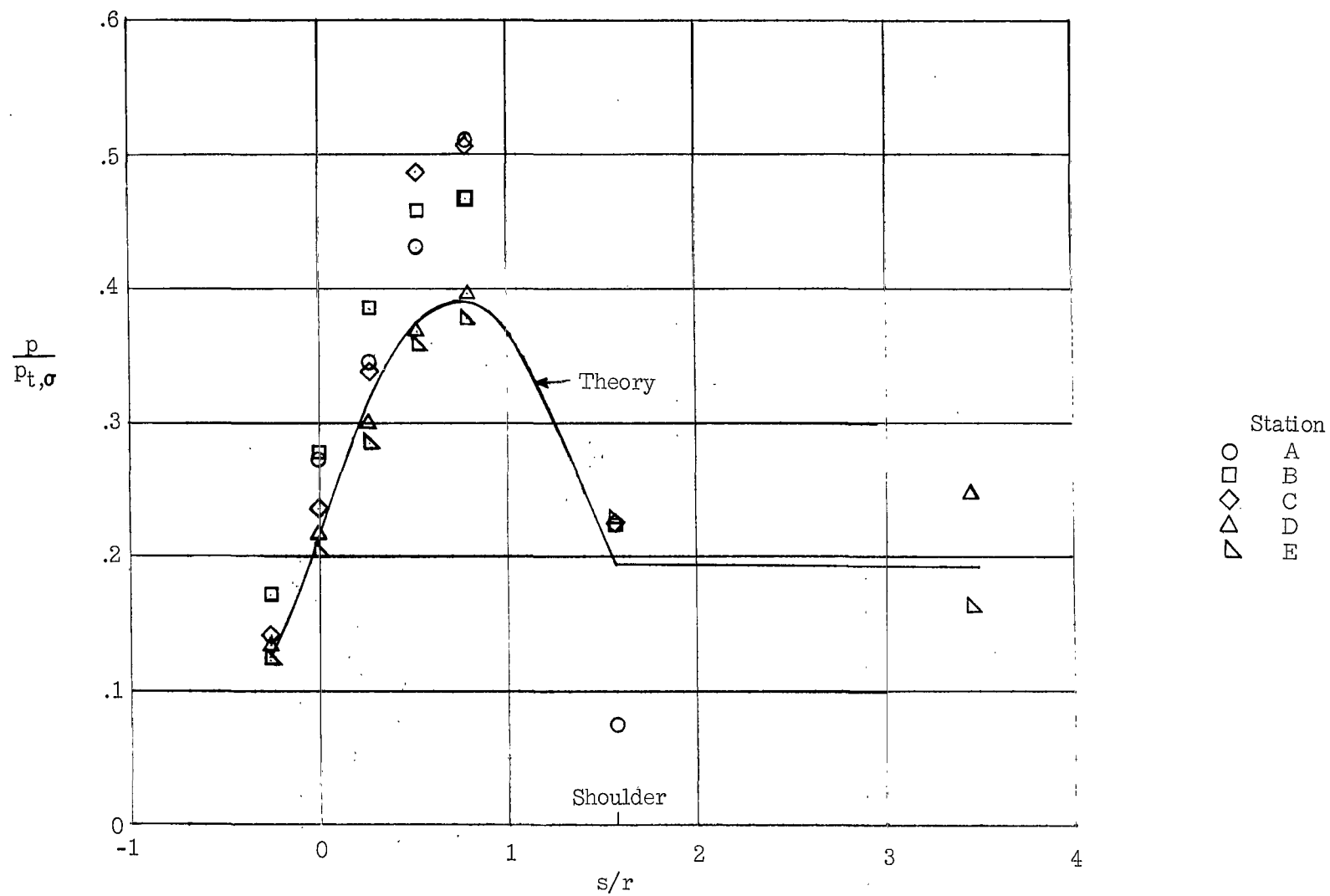
Figure 5.- Continued.

(f) $\beta = 25^{\circ}$.

Figure 5.- Continued.
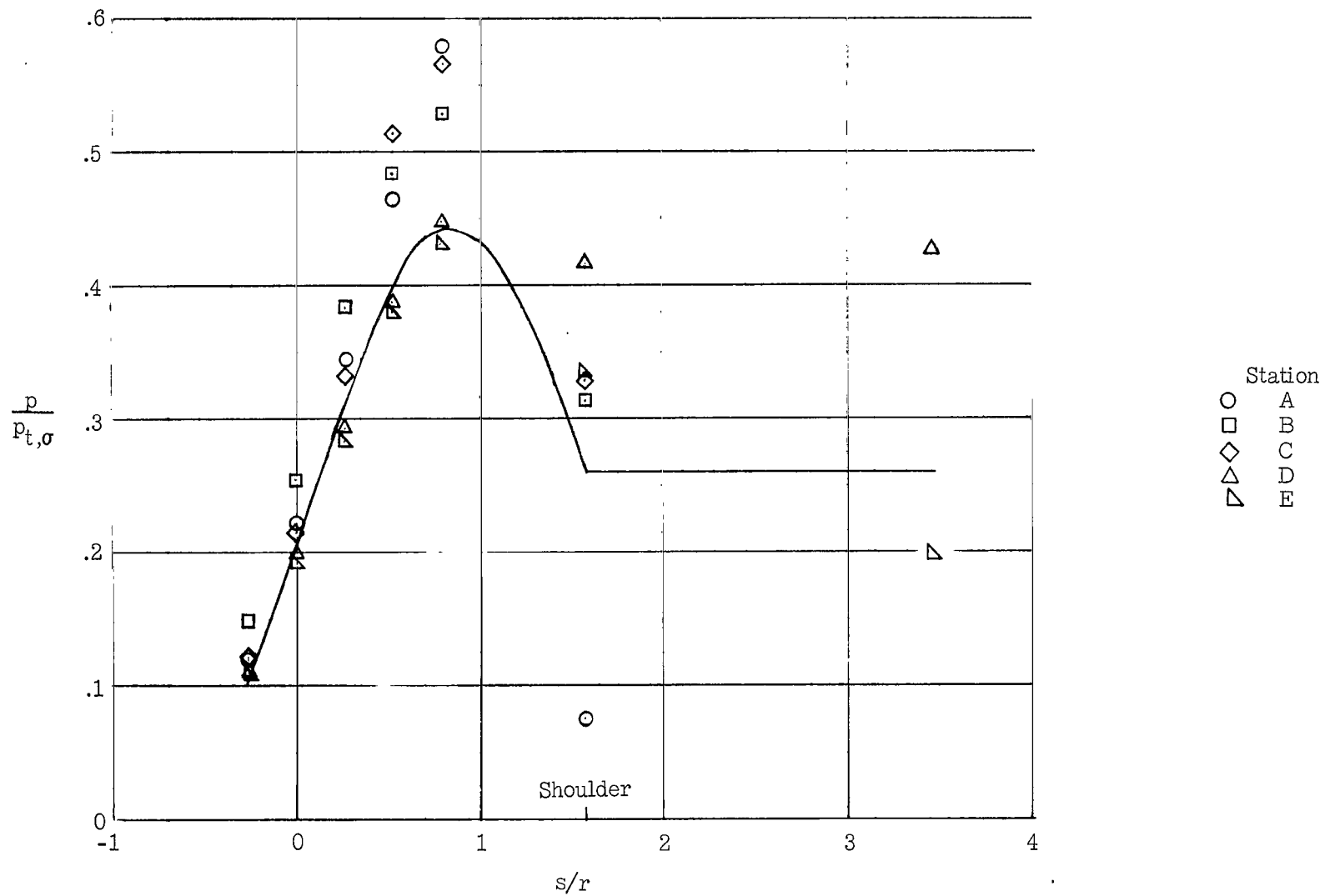
(g) $\beta = 30°$.

Figure 5.- Concluded.
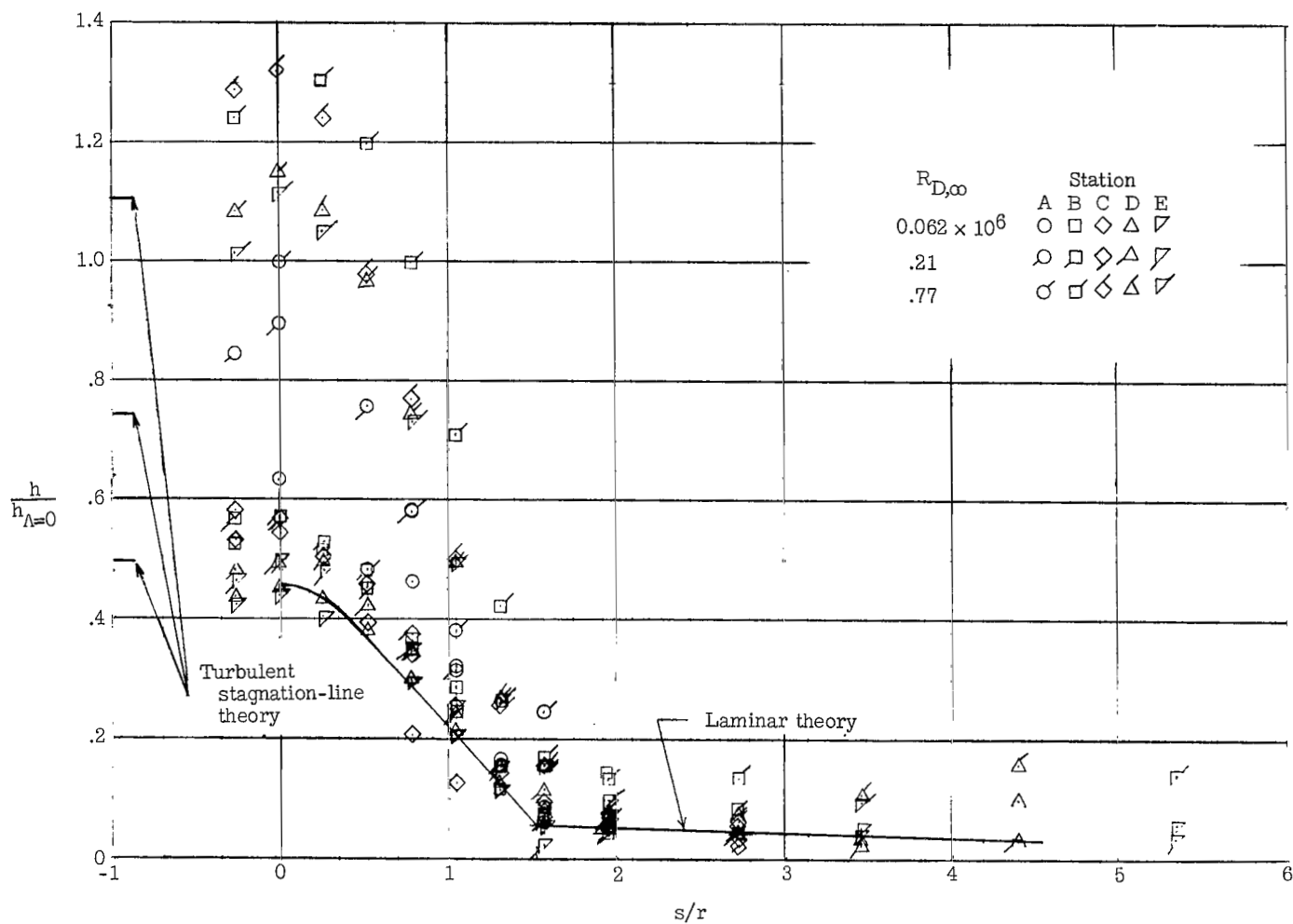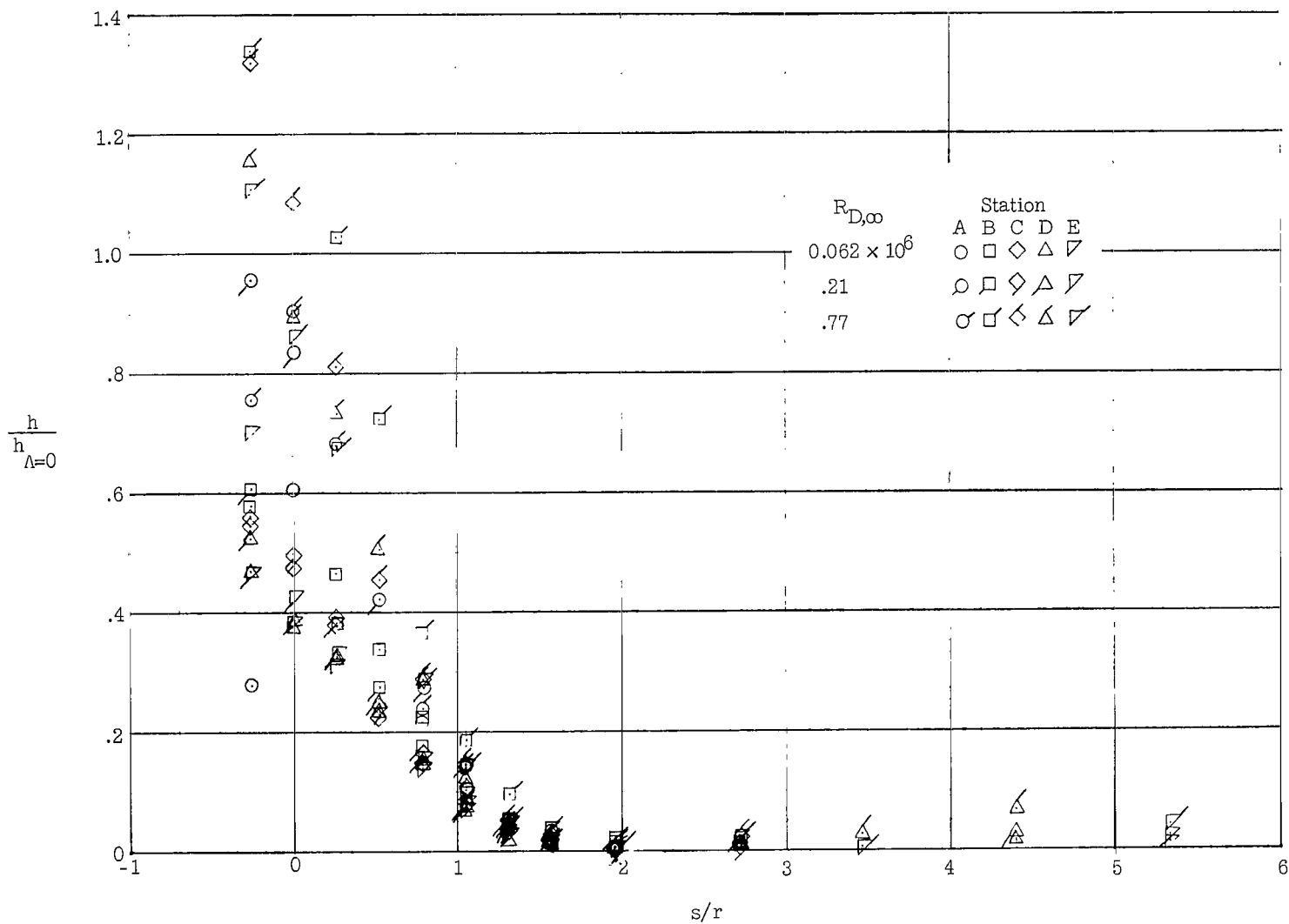
(a) β = 0°.

Figure 6.- Heat-transfer distribution on fin (windward side).
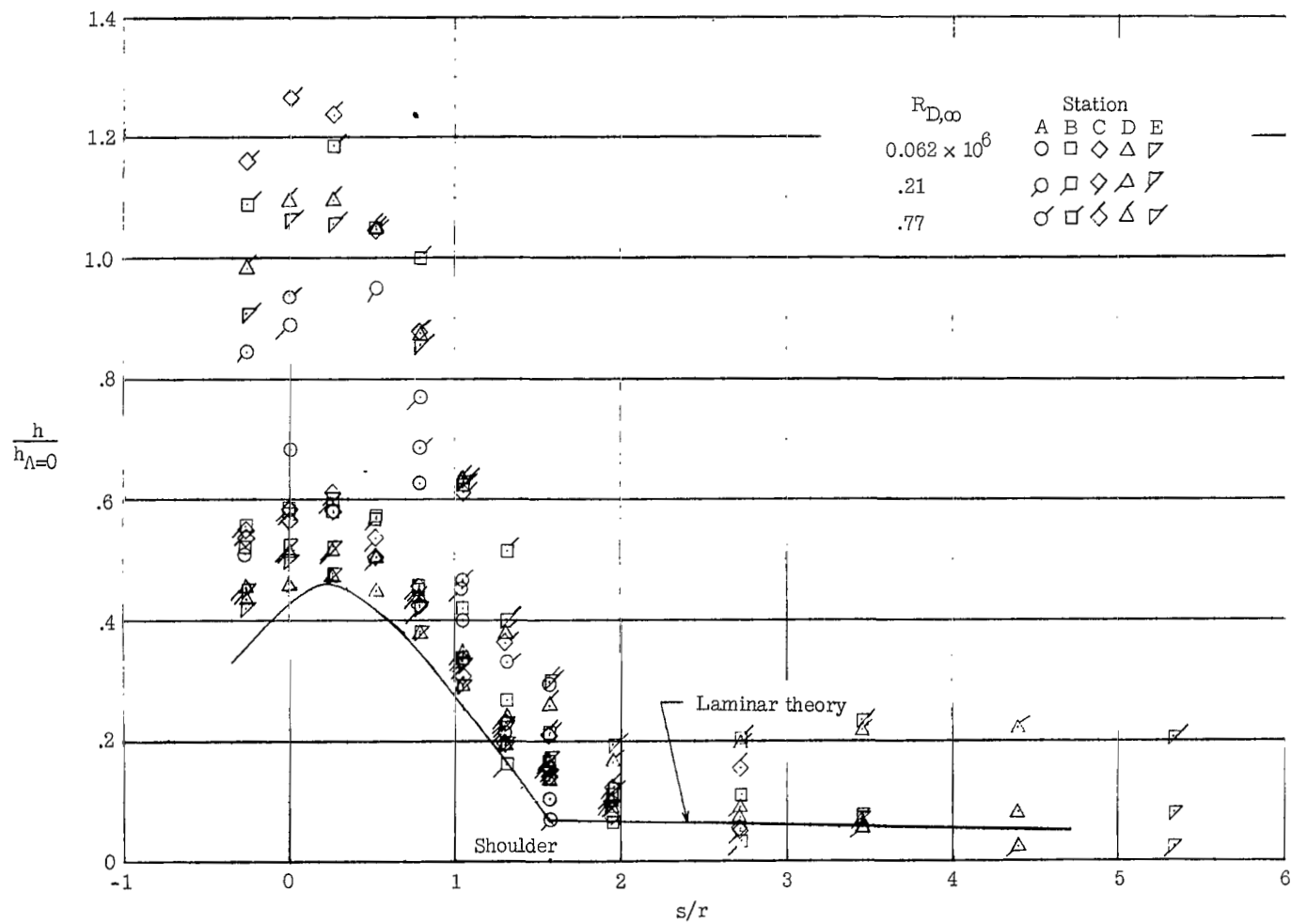
(b) $\beta = 5^{\circ}$.

Figure 6.- Continued.
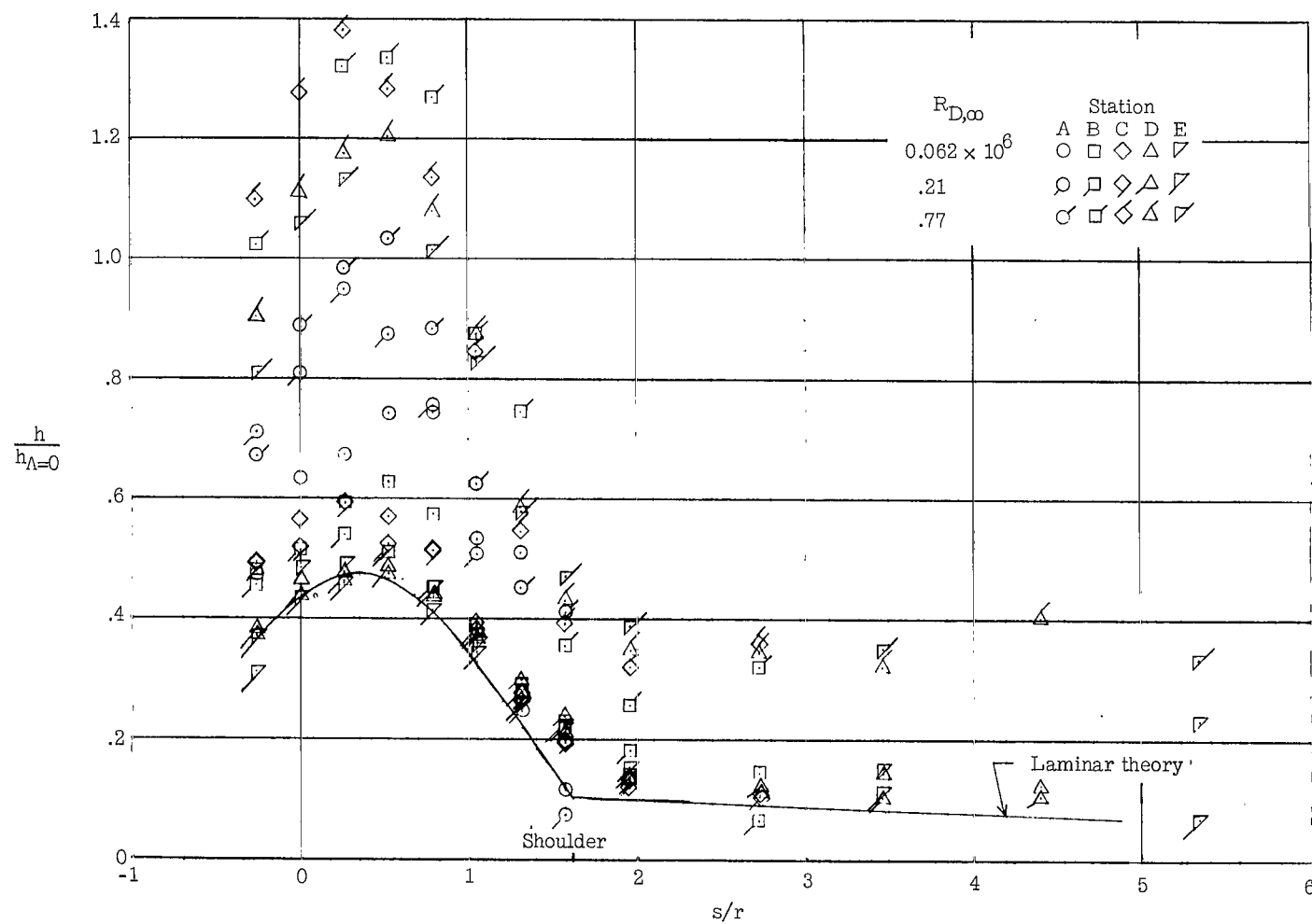
(c) $\beta = 10°$.

Figure 6.- Continued.
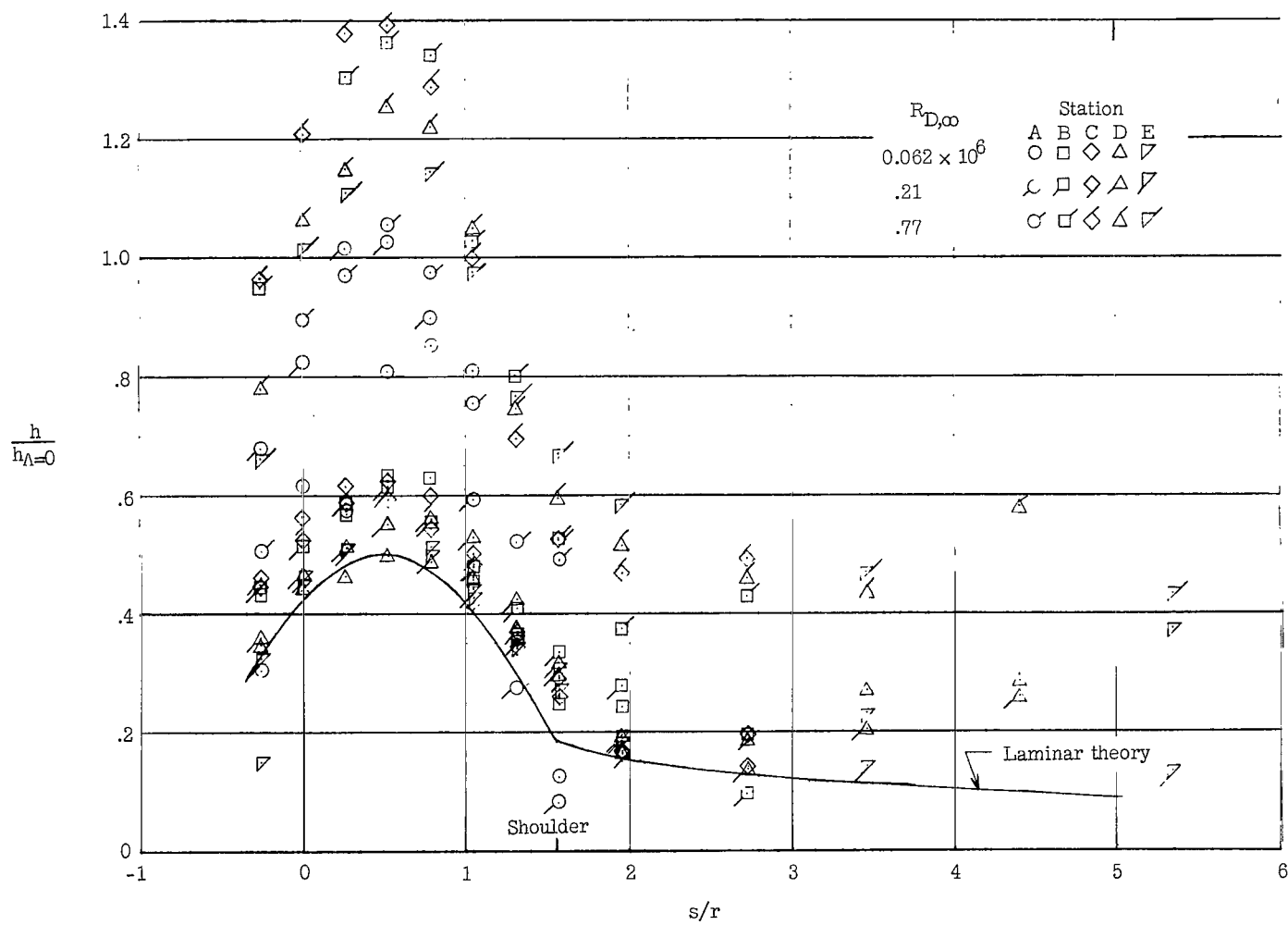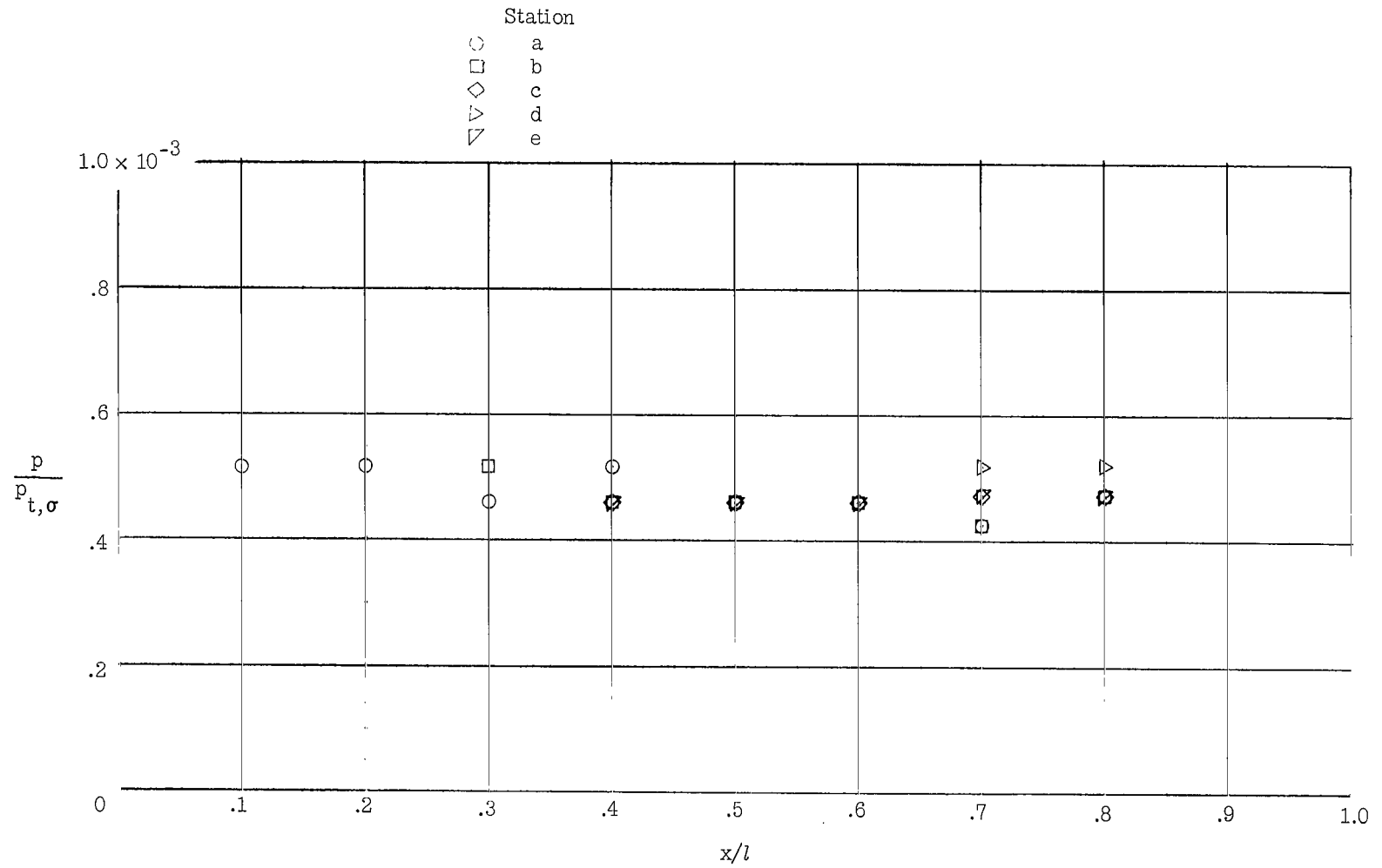
(d) $\beta = 15°$.

Figure 6.- Continued.
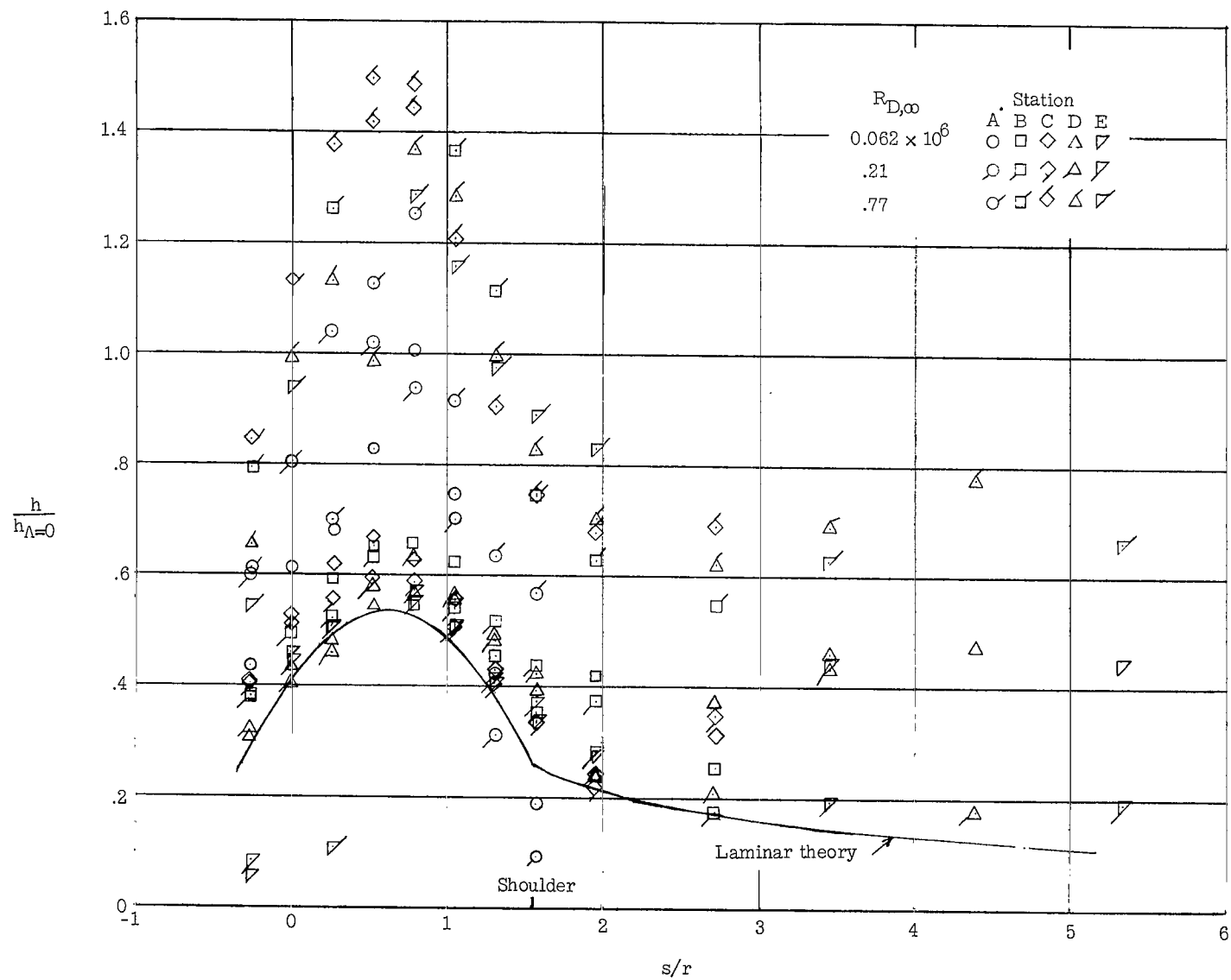
(e) $\beta = 20^\circ$.

Figure 6.- Continued.
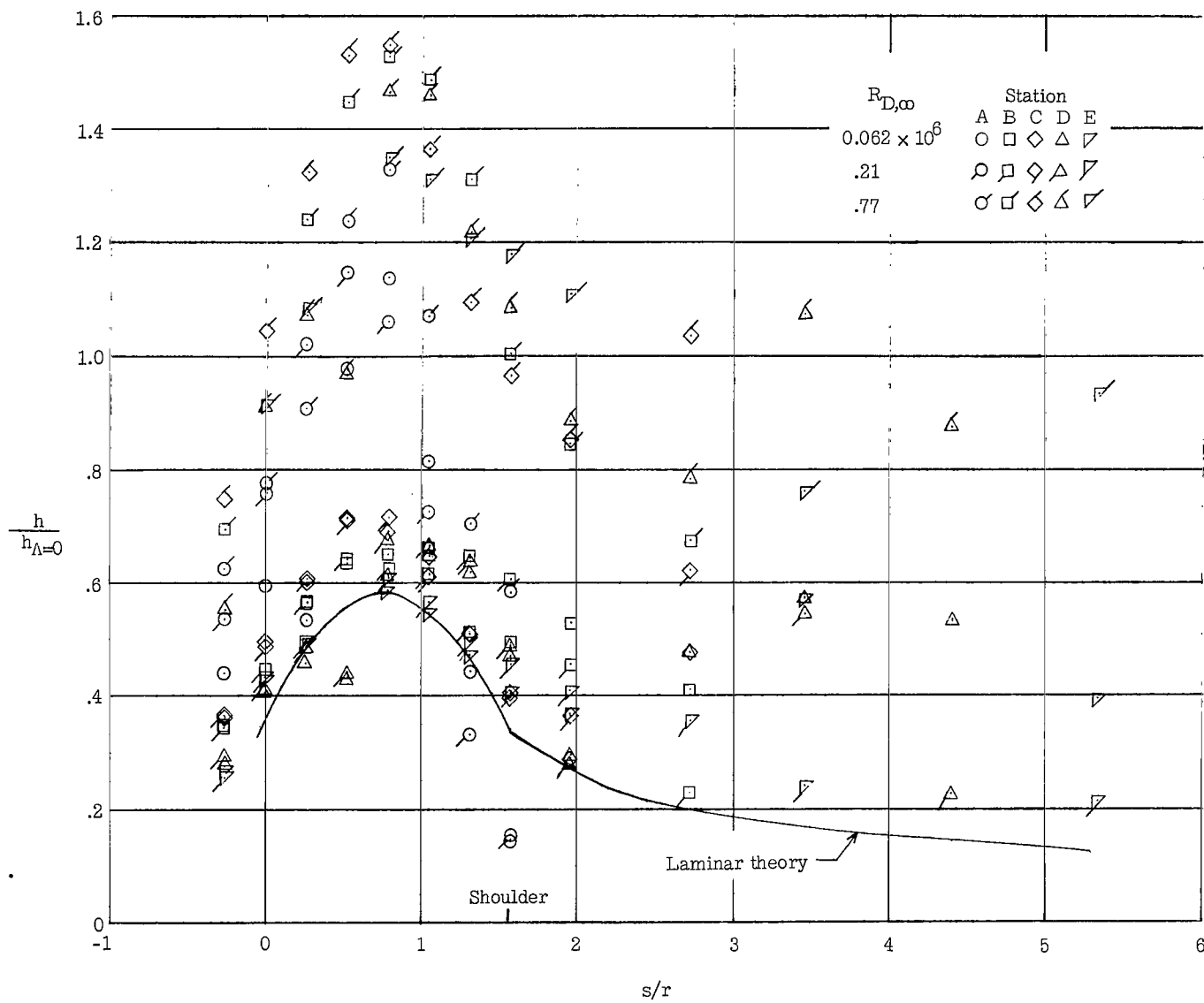
(f) $\beta = 25°$.

Figure 6.- Continued.
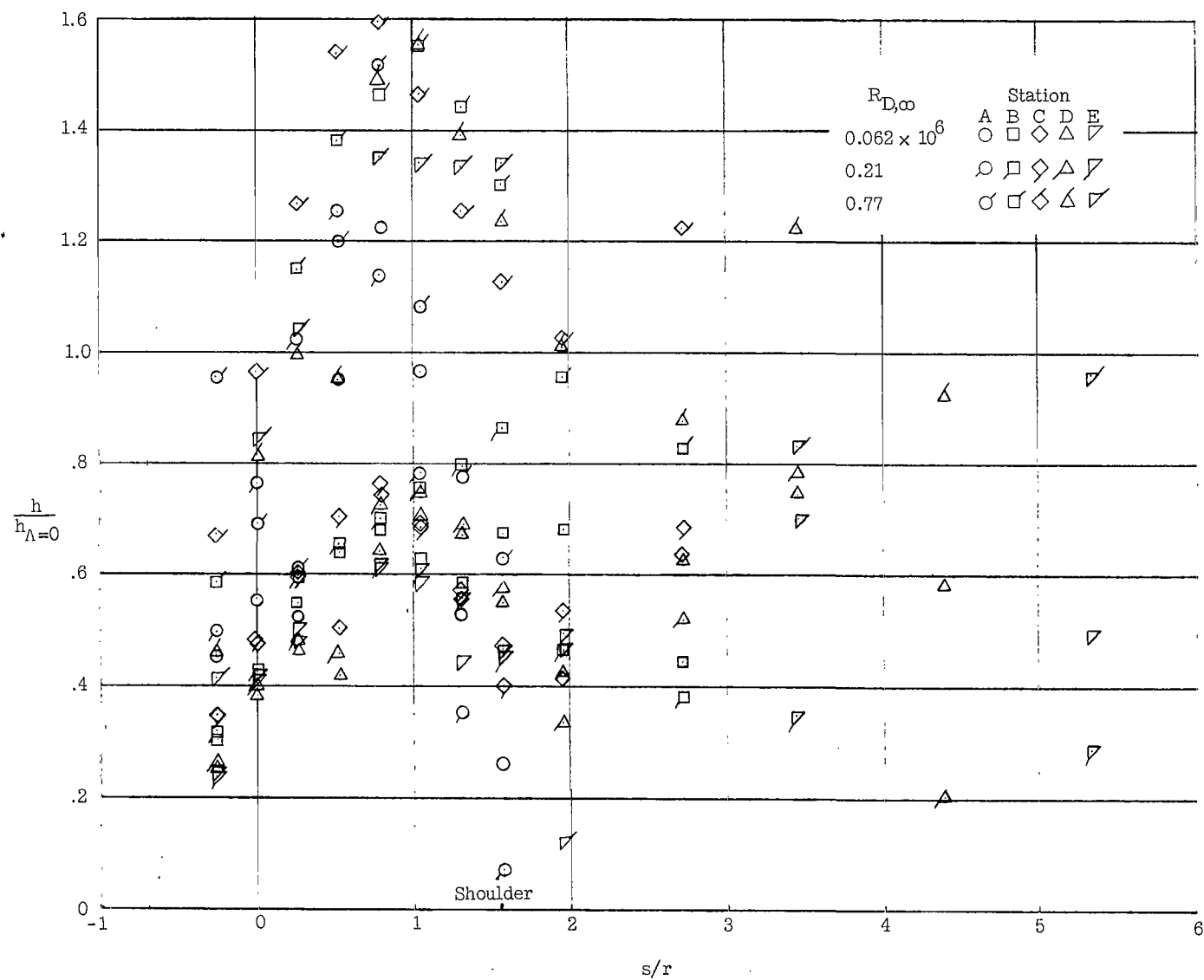
(g) $\beta = 30°$.

Figure 6.- Concluded.
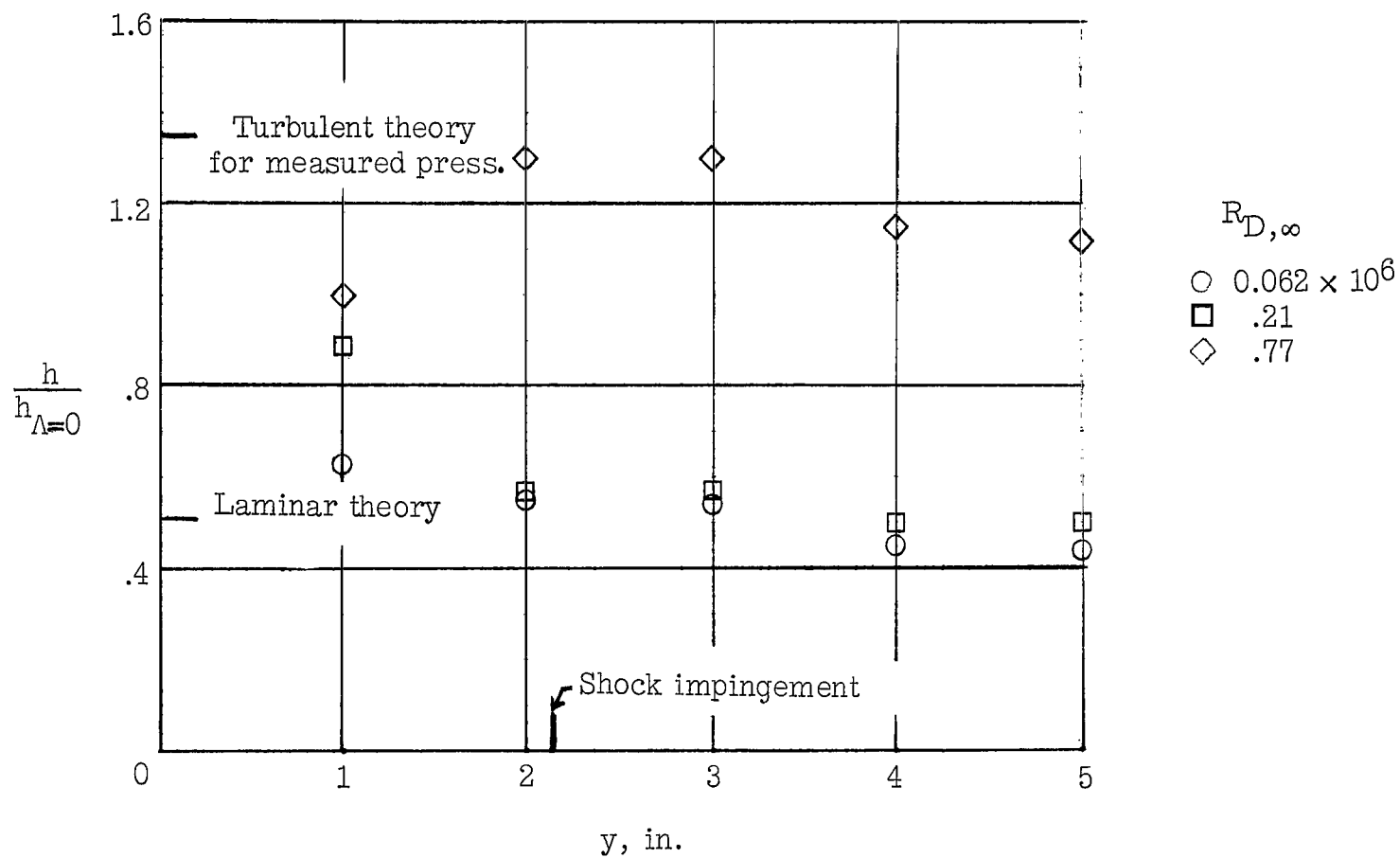
(a) $\beta = 0^\circ$.

Figure 7.- Heat-transfer distribution along stagnation line of fin.

(b) $\beta = 25^\circ$.

Figure 7.- Concluded.

1.4

1.2

1.0

.8

$\dfrac{h}{h_{\Lambda=0}}$

.6

.4

.2

0

		Station
$R_{D,\infty}$		A B C D E
0.062×10^6		○ □ ◇ △ ▽
.21		◐ ◭ ◈ ⟁ ⟆
.77		◑ ◩ ◆ ◮ ⟈

-1   0   1   2   3   4   5   6

s/r
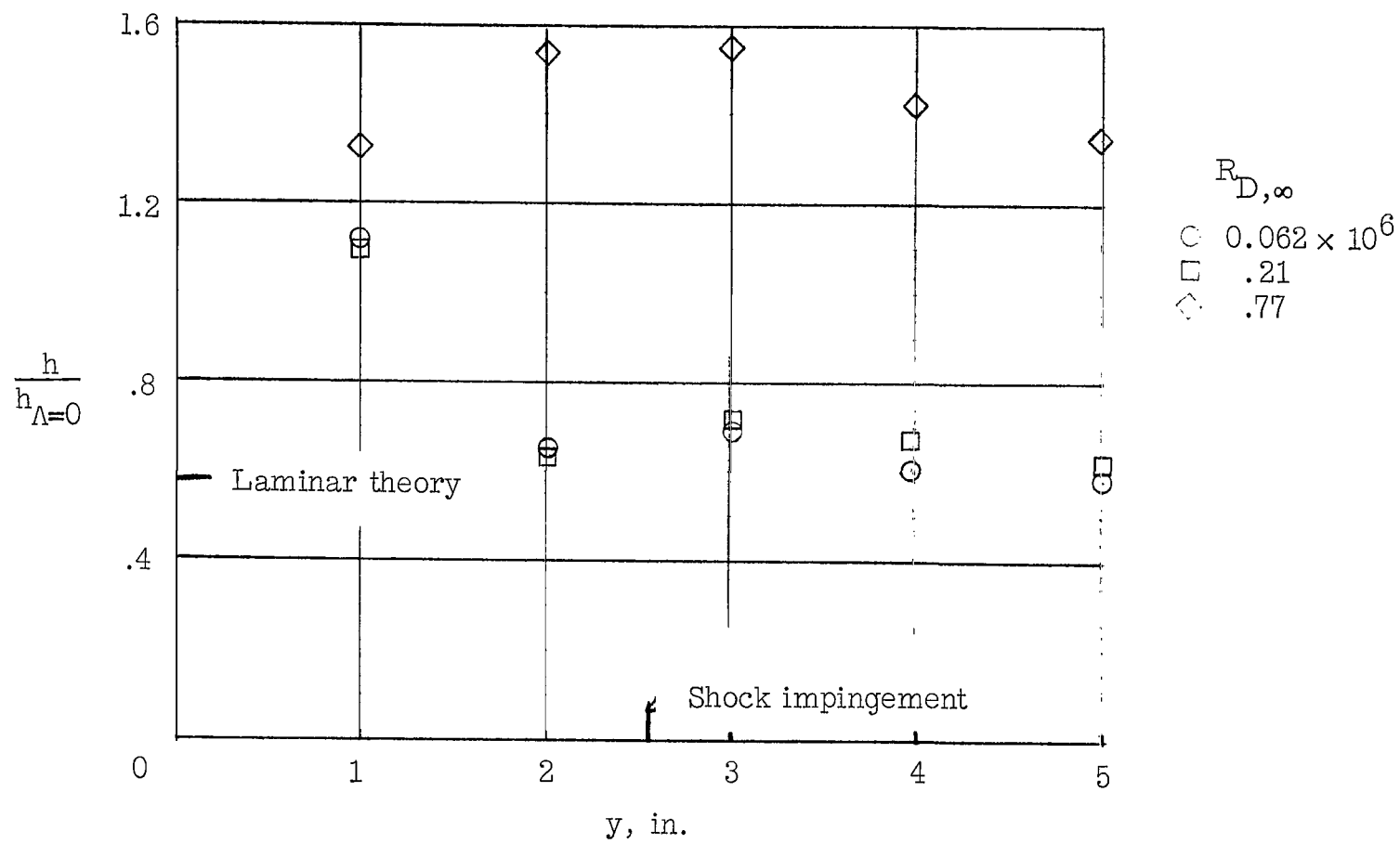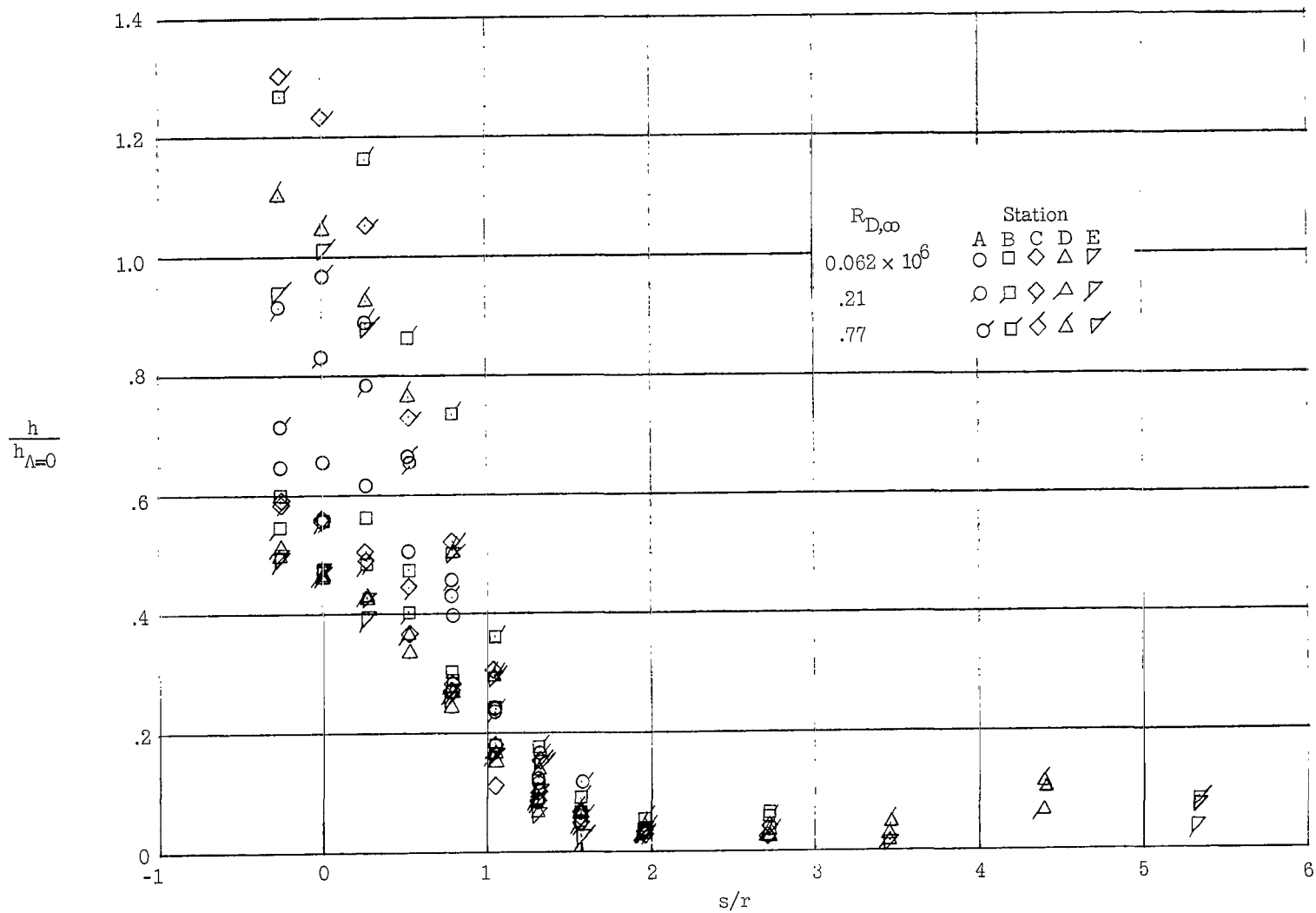
(a) β = -5°.

Figure 8.- Heat-transfer distribution on fin (leeward side).
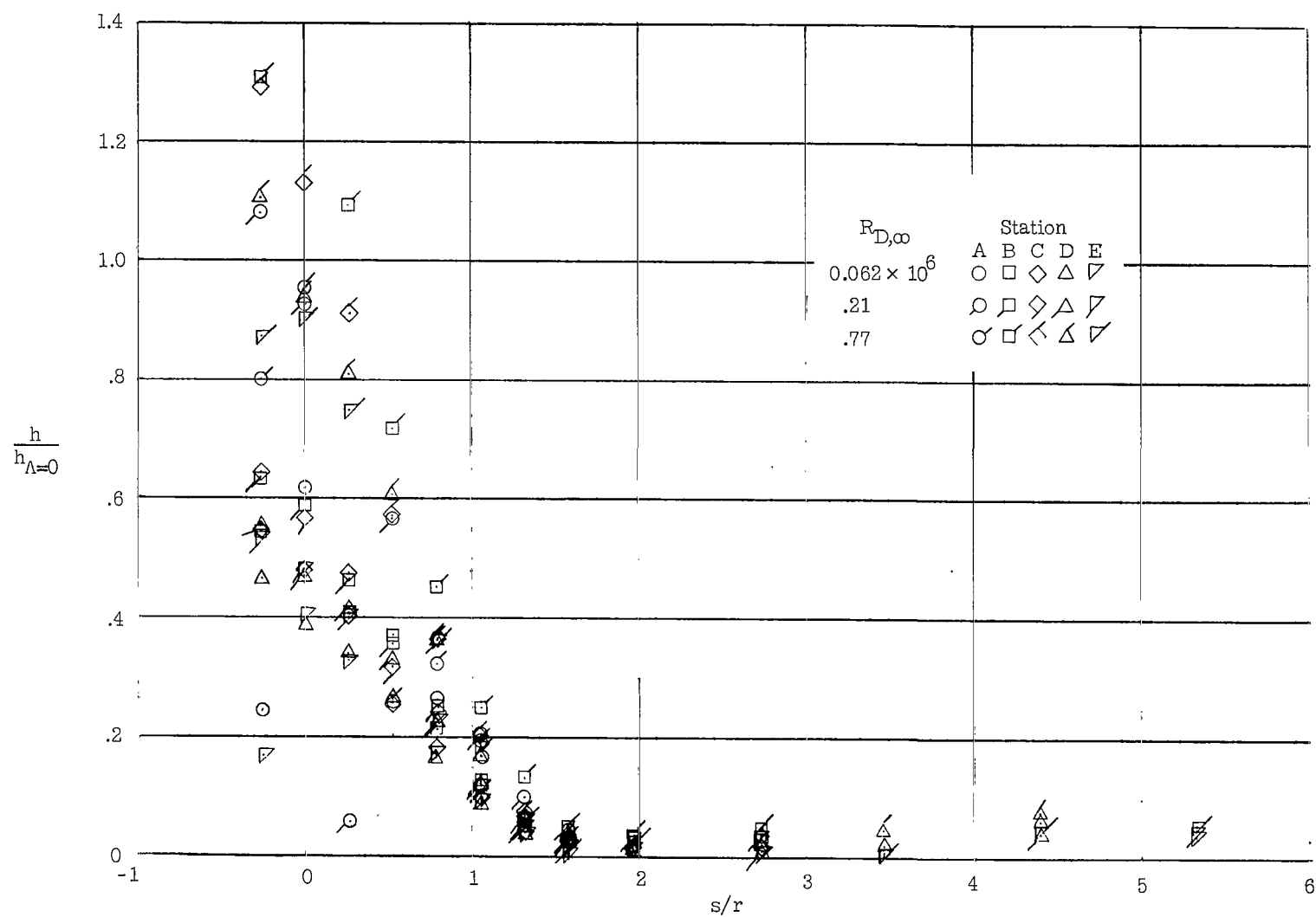
(b) β = -10°.

Figure 8.- Continued.

(c) $\beta = -15°$.

Figure 8.- Concluded.

Station
○   a
□   b
◇   c
▷   d
▽   e

$\dfrac{p}{p_{t,\sigma}}$

1.0×10^{-3}

.8

.6

.4

.2

0

.1   .2   .3   .4   .5   .6   .7   .8   .9   1.0

x/l

Figure 9.- Pressures on plate without fin. $R_{D,\infty} = 0.70 \times 10^{6}$.
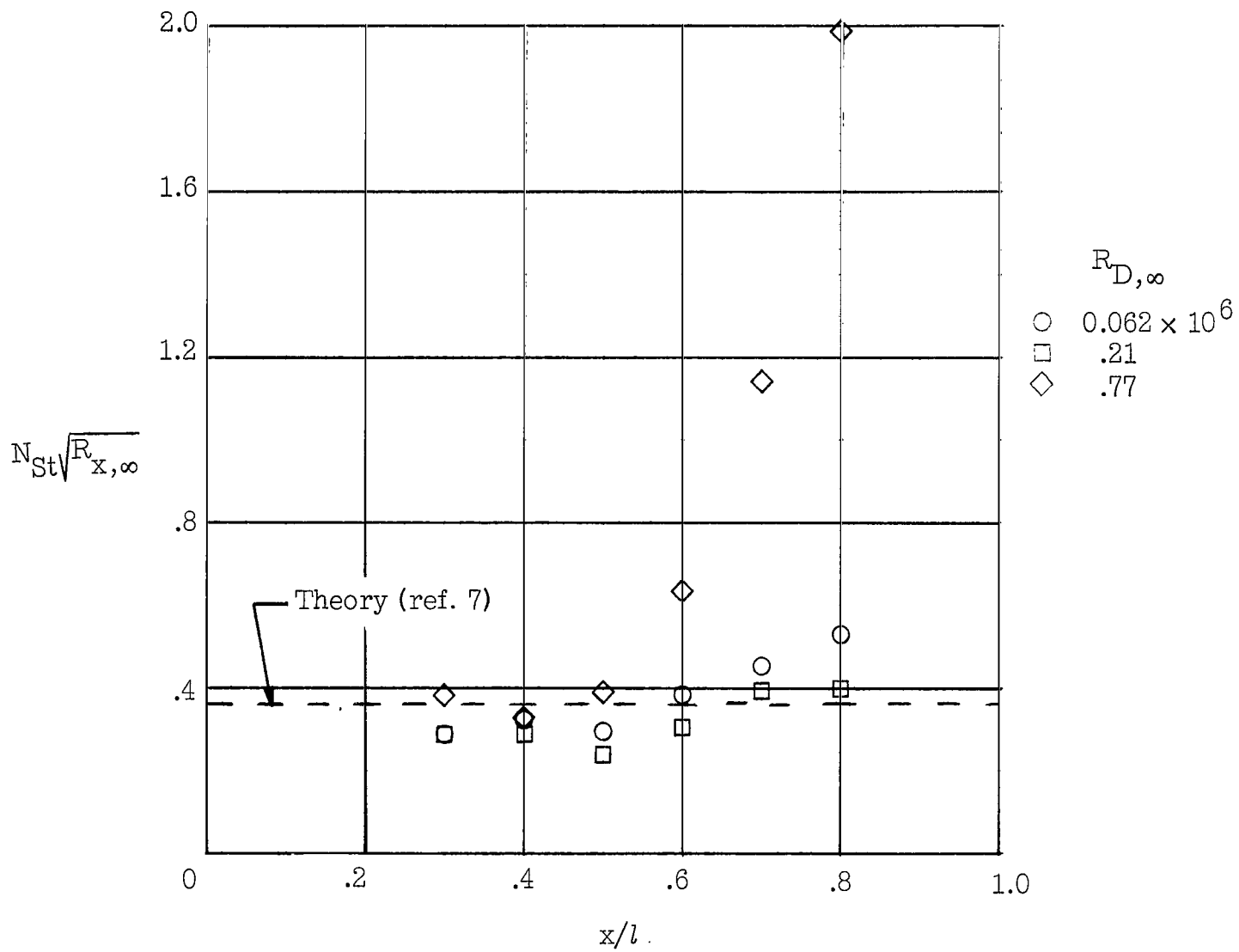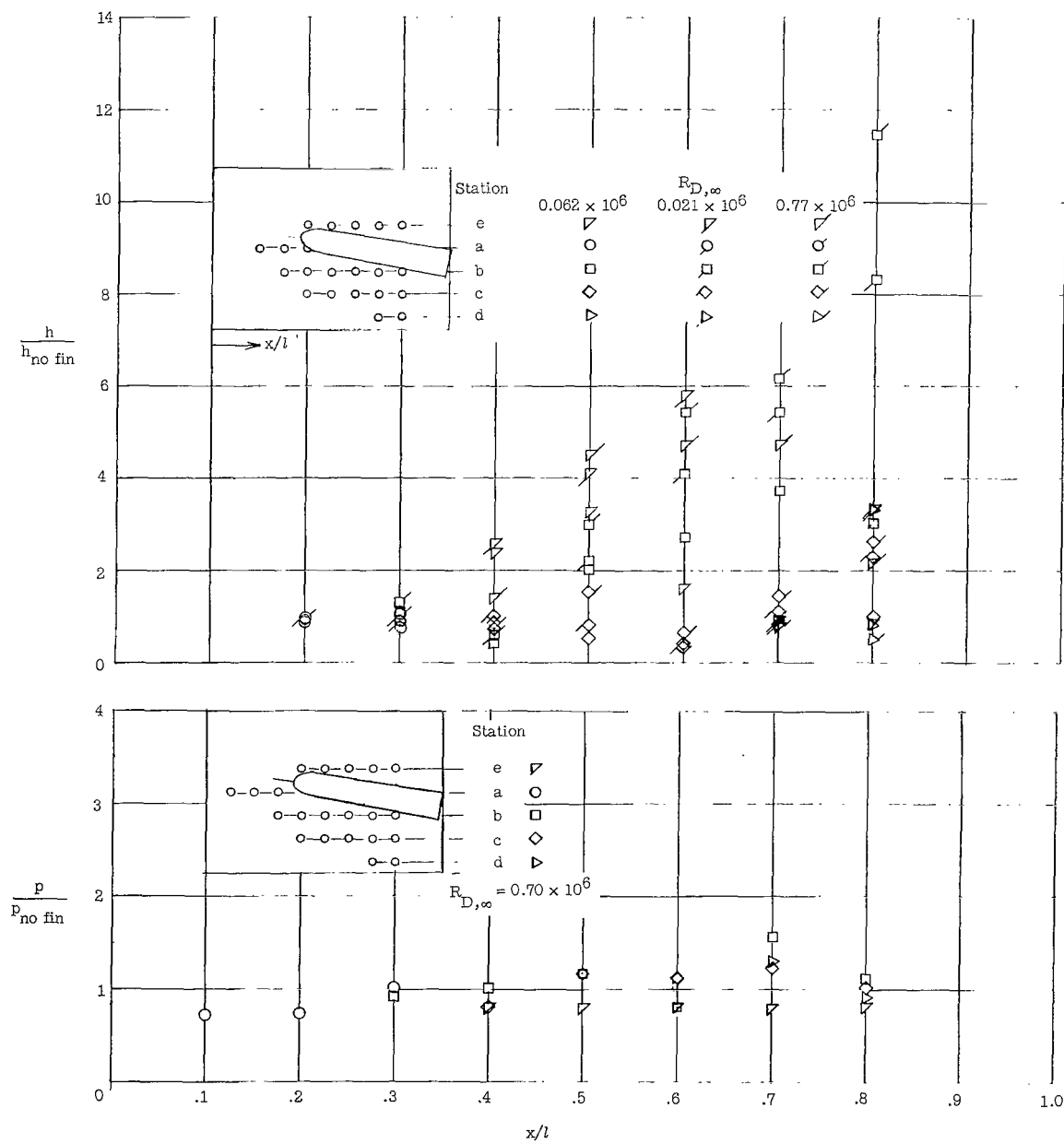
Figure 10.- Heat transfer to plate without fin.
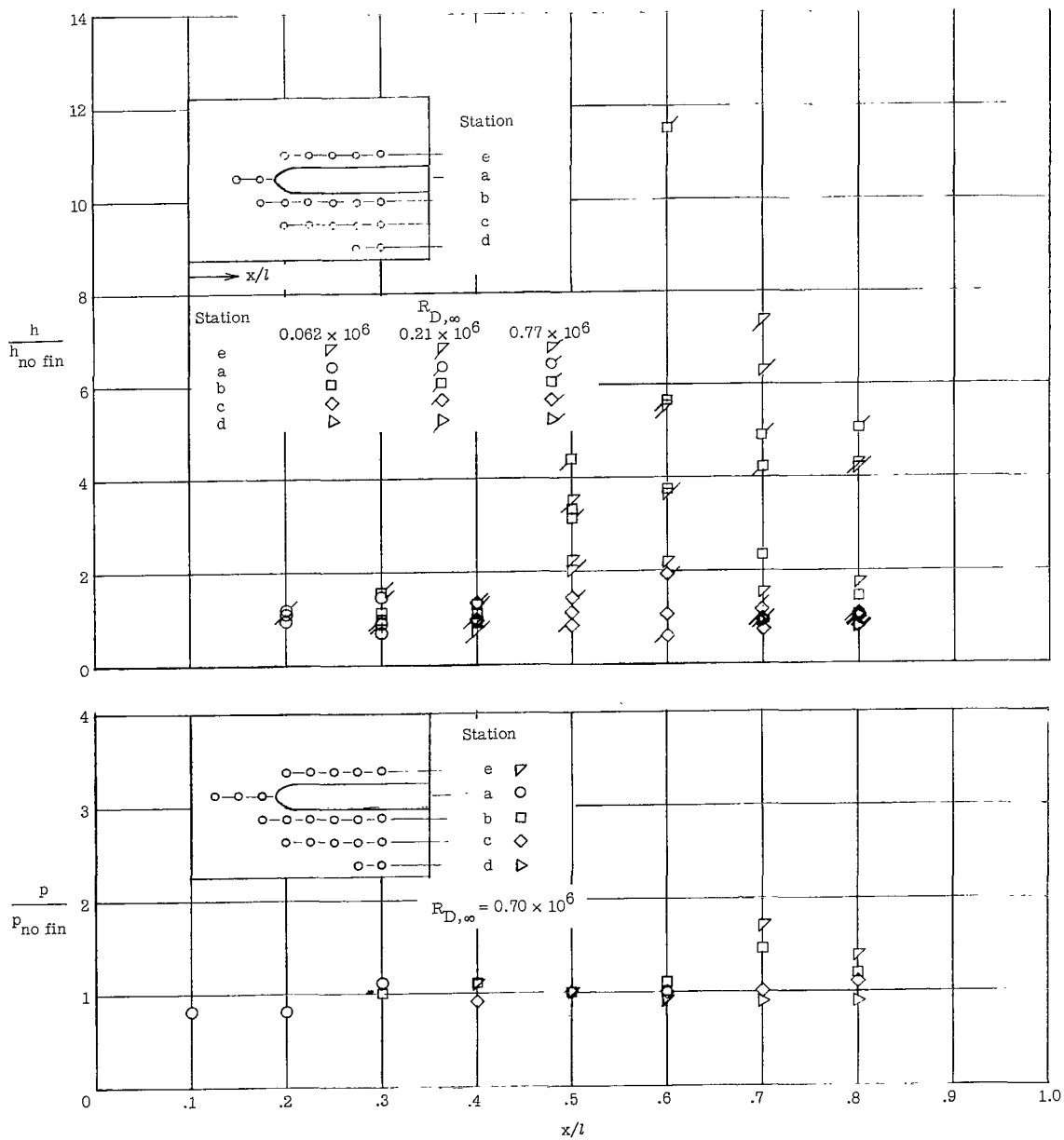
(a) β = 0°.

Figure 11.- Pressure and heat-transfer distribution on plate.
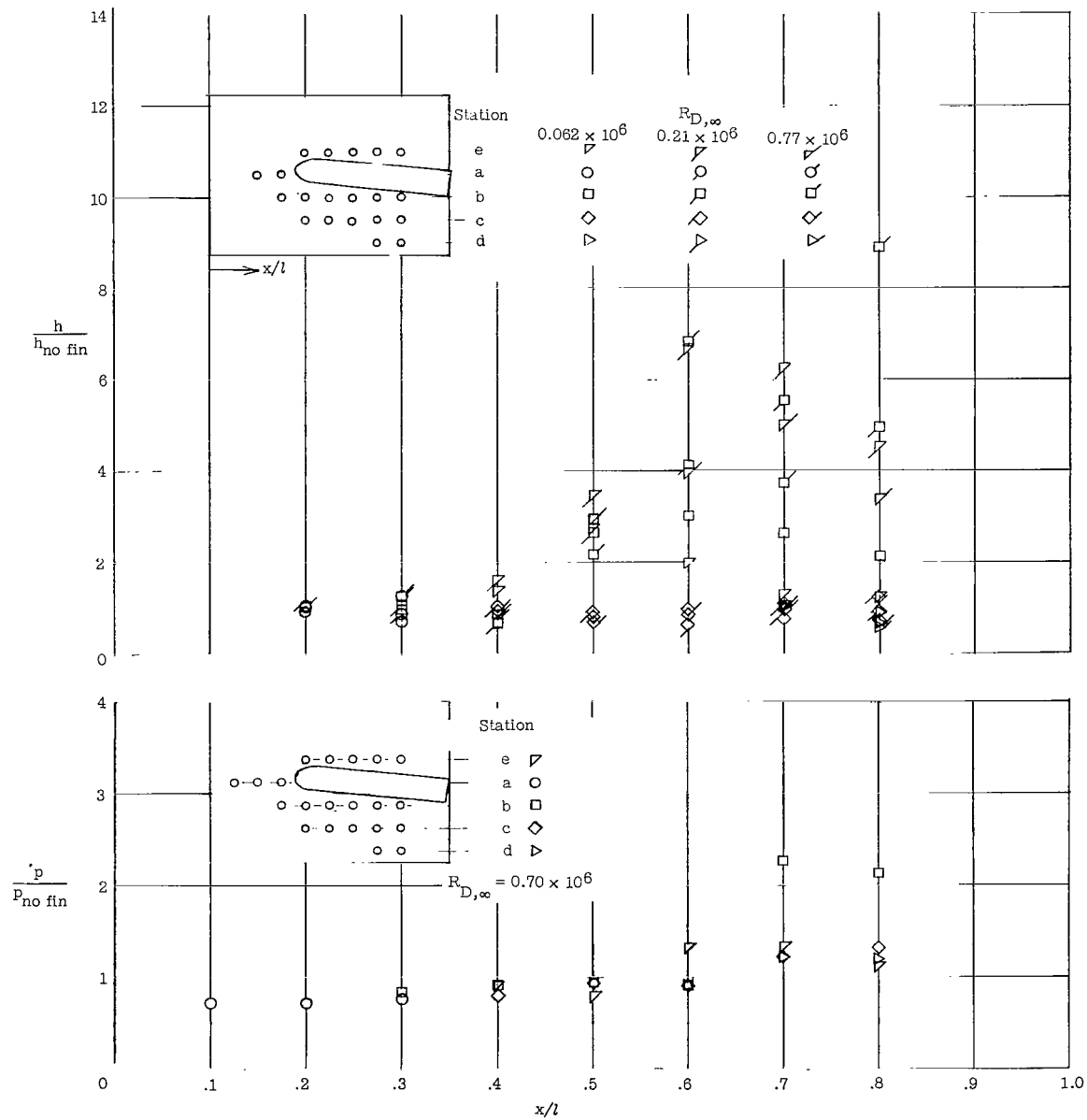
(b) $\beta = 5°$.

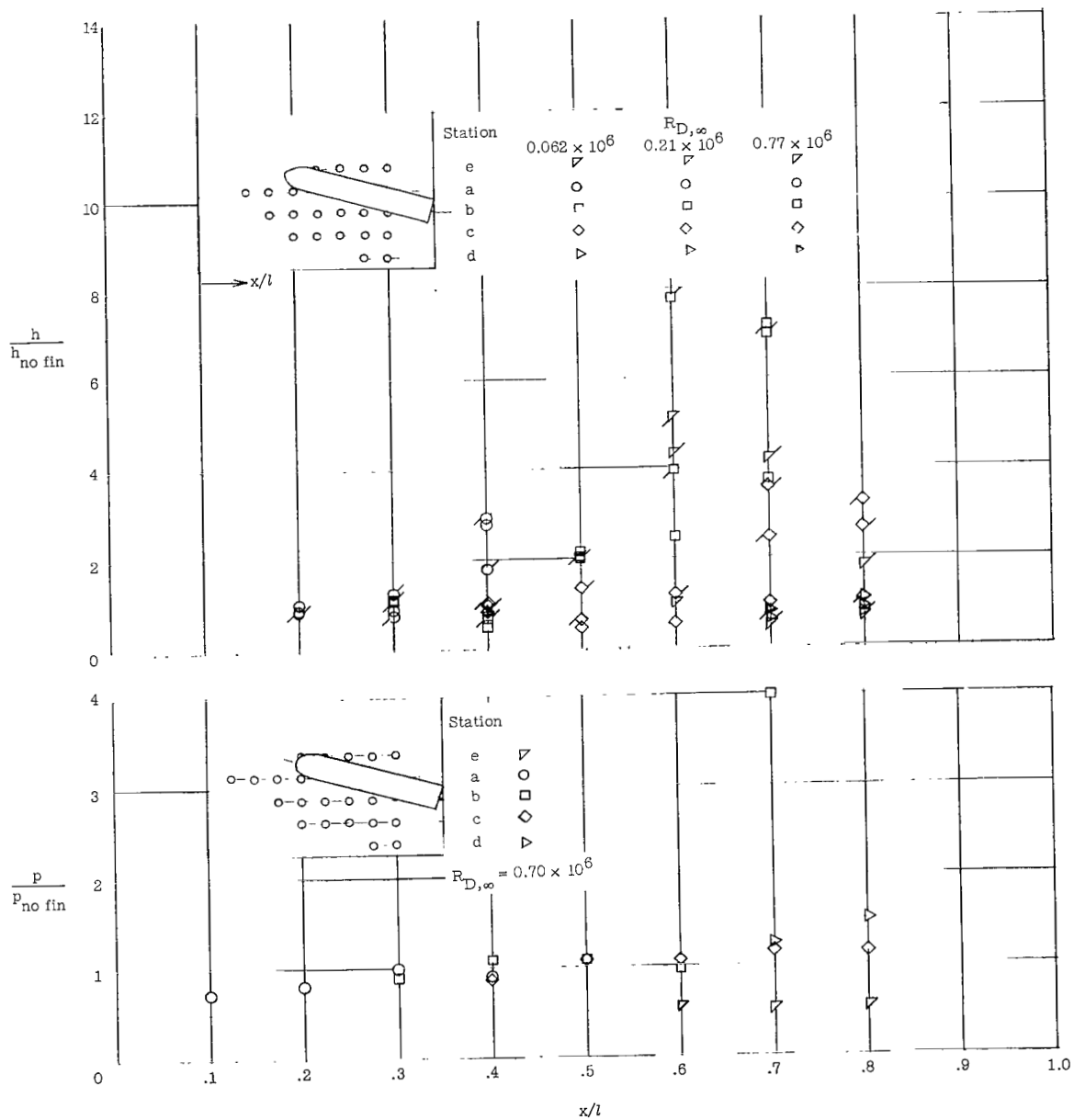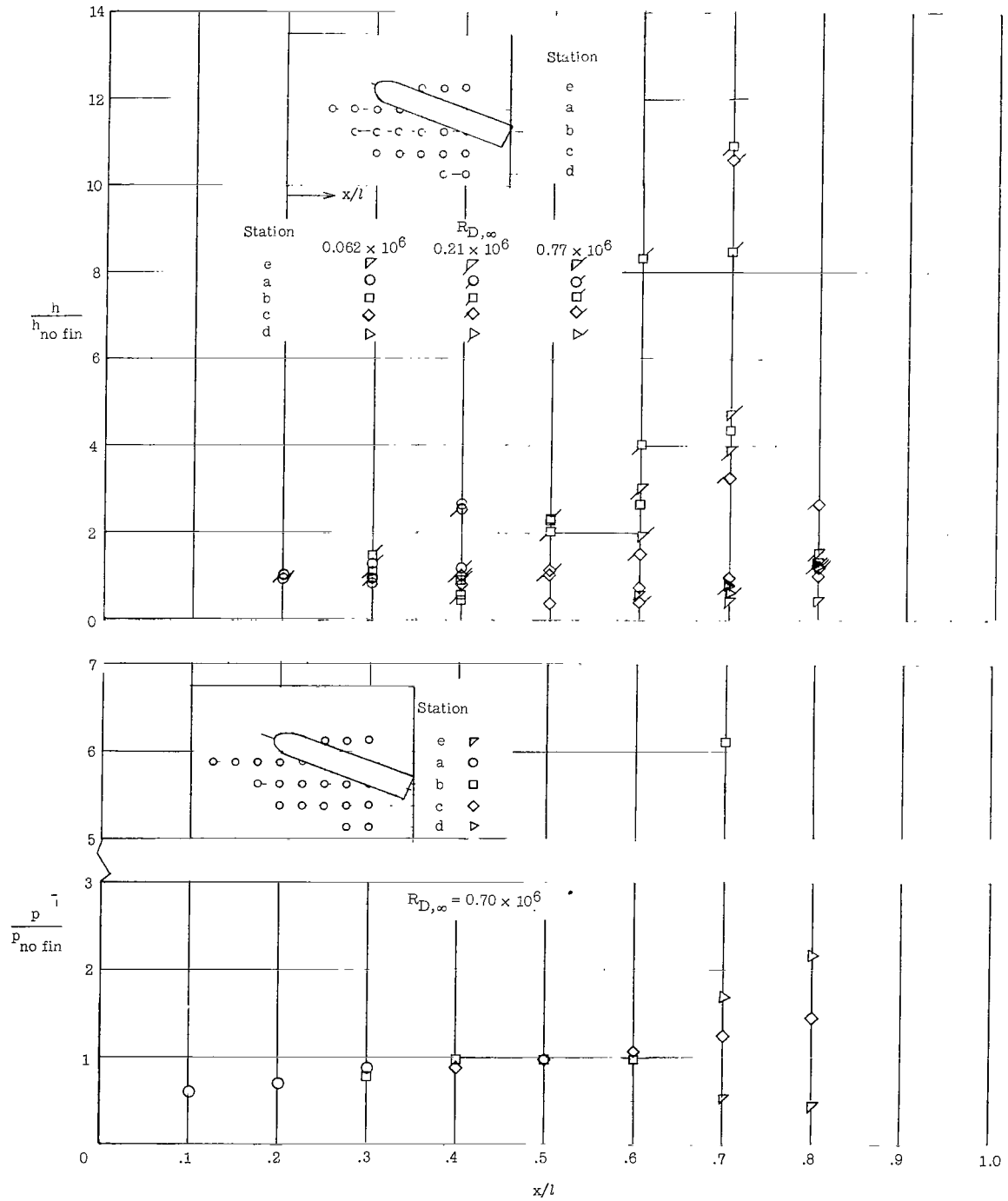Figure 11.- Continued.

39

(c) $\beta = 10^{\circ}$.
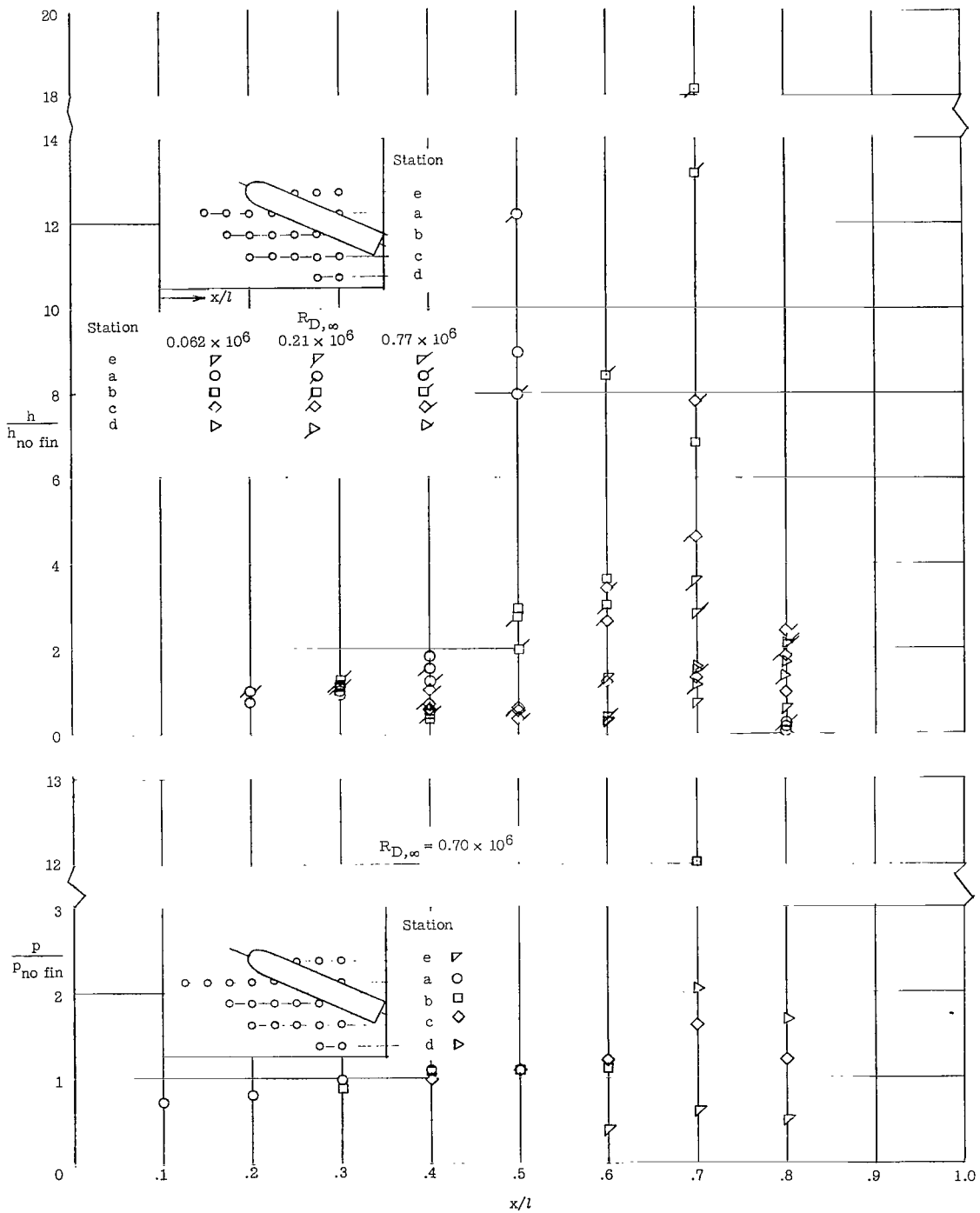
Figure 11.- Continued.

(d) β = 15°.

Figure 11.- Continued.

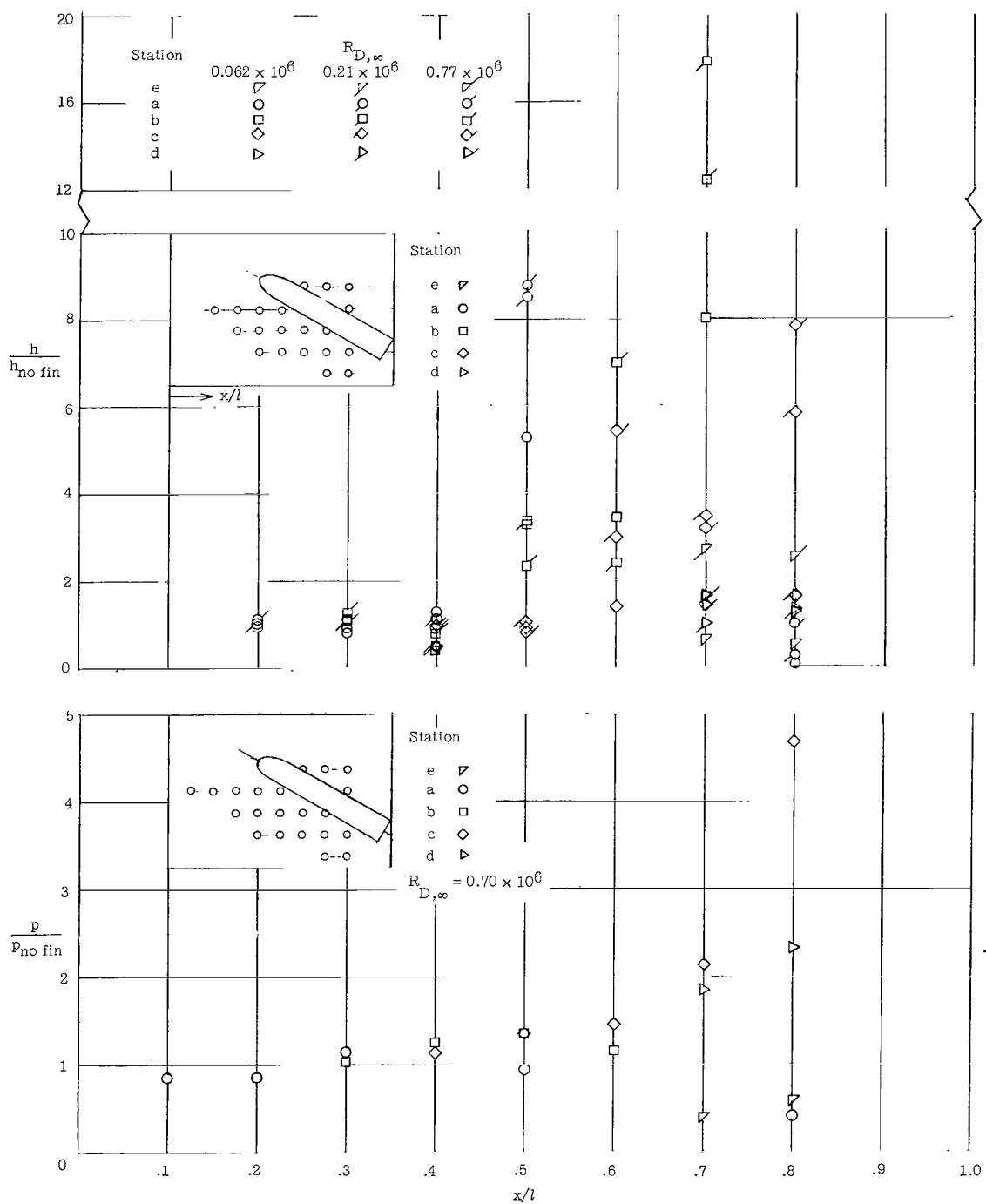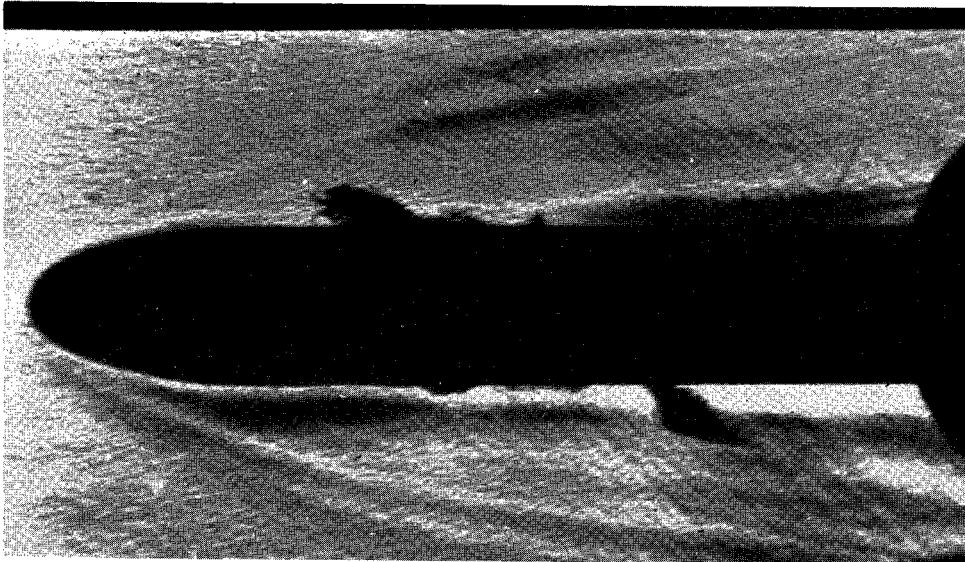(e) $\beta = 20^{\circ}$.

Figure 11.- Continued.

20

18

14

12

10

$\dfrac{h}{h_{\text{no fin}}}$

8

6

4

2

0

Station

e
a
b
c
d

$\begin{array}{c} \text{Station} \\ \text{e} \\ \text{a} \\ \text{b} \\ \text{c} \\ \text{d} \end{array}$

$R_{D,\infty}$

$0.062 \times 10^6 \qquad 0.21 \times 10^6 \qquad 0.77 \times 10^6$

x/l

13

12

3

$\dfrac{p}{p_{\text{no fin}}}$

2

1

0

$R_{D,\infty} = 0.70 \times 10^6$

Station

e ▽
a ○
b □
c ◇
d ▷

0   .1   .2   .3   .4   .5   .6   .7   .8   .9   1.0

x/l

(f) $\beta = 25°$.
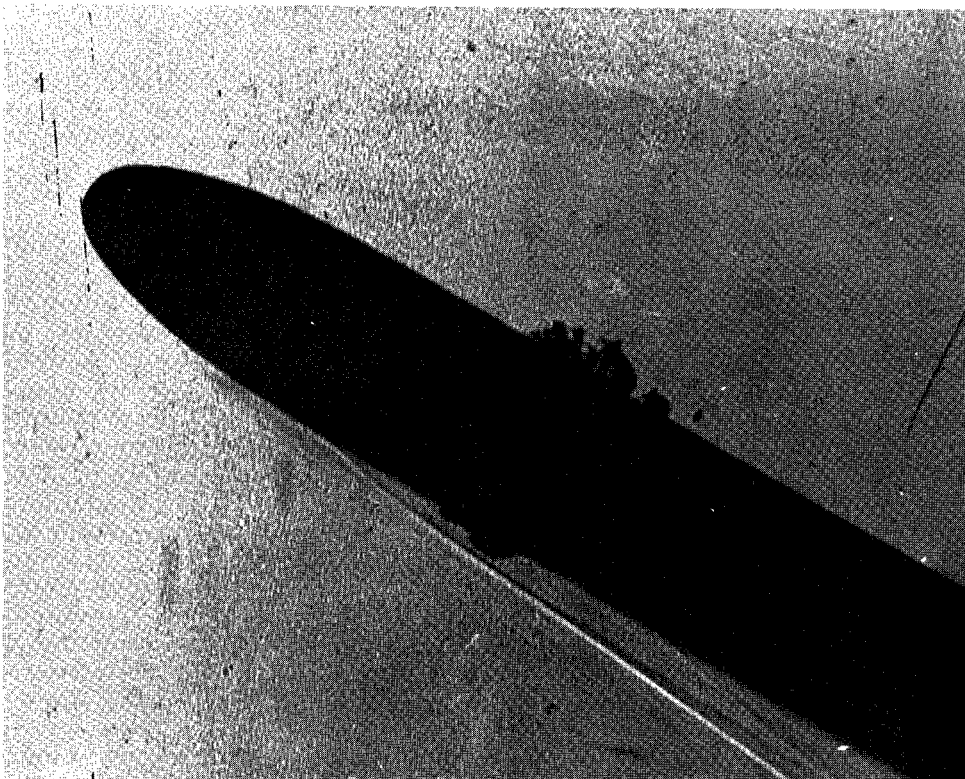
Figure 11.- Continued.

43

(g) β = 30°.

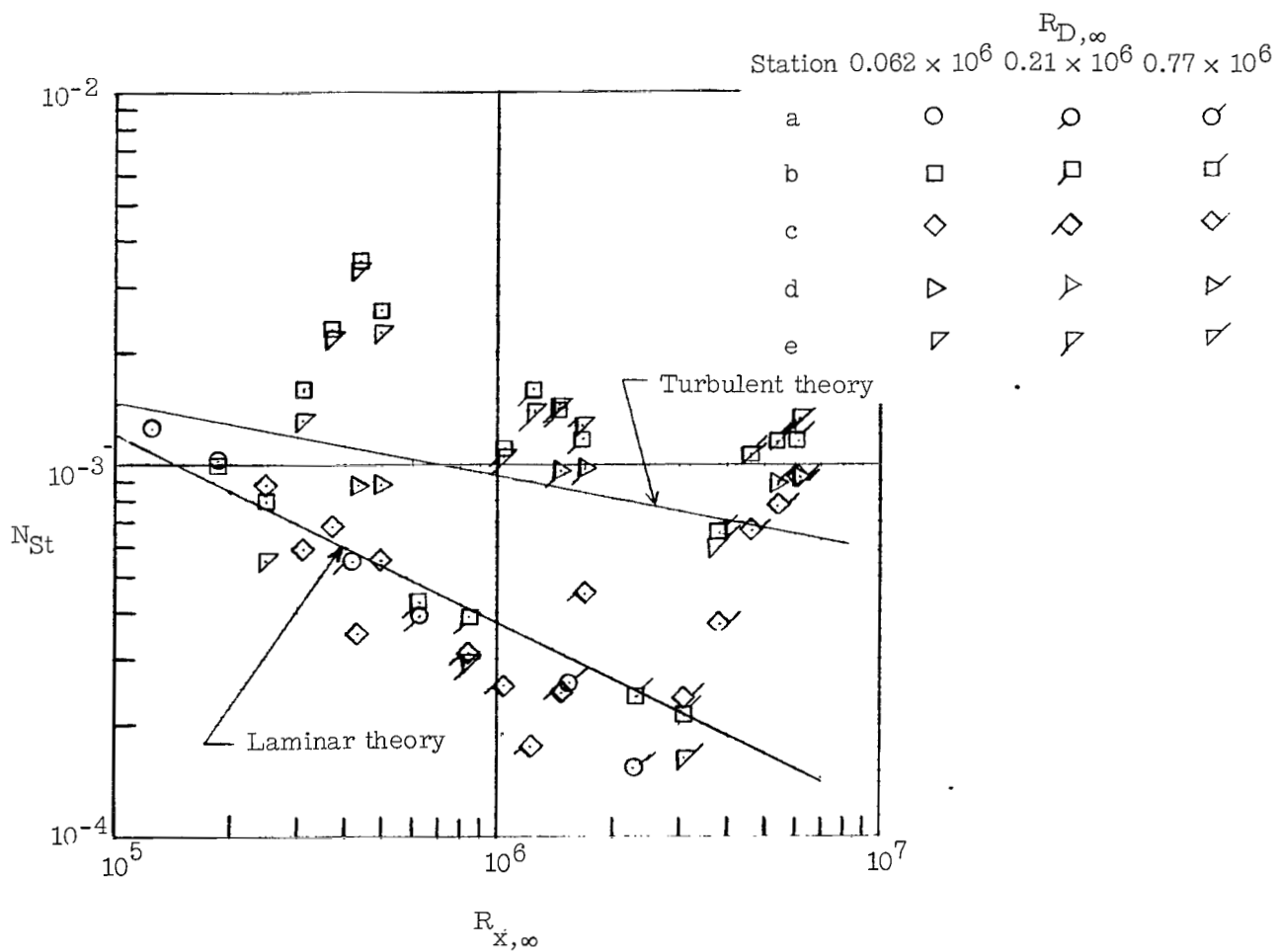Figure 11.- Concluded.

(a) $\beta = 0^{\circ}$.
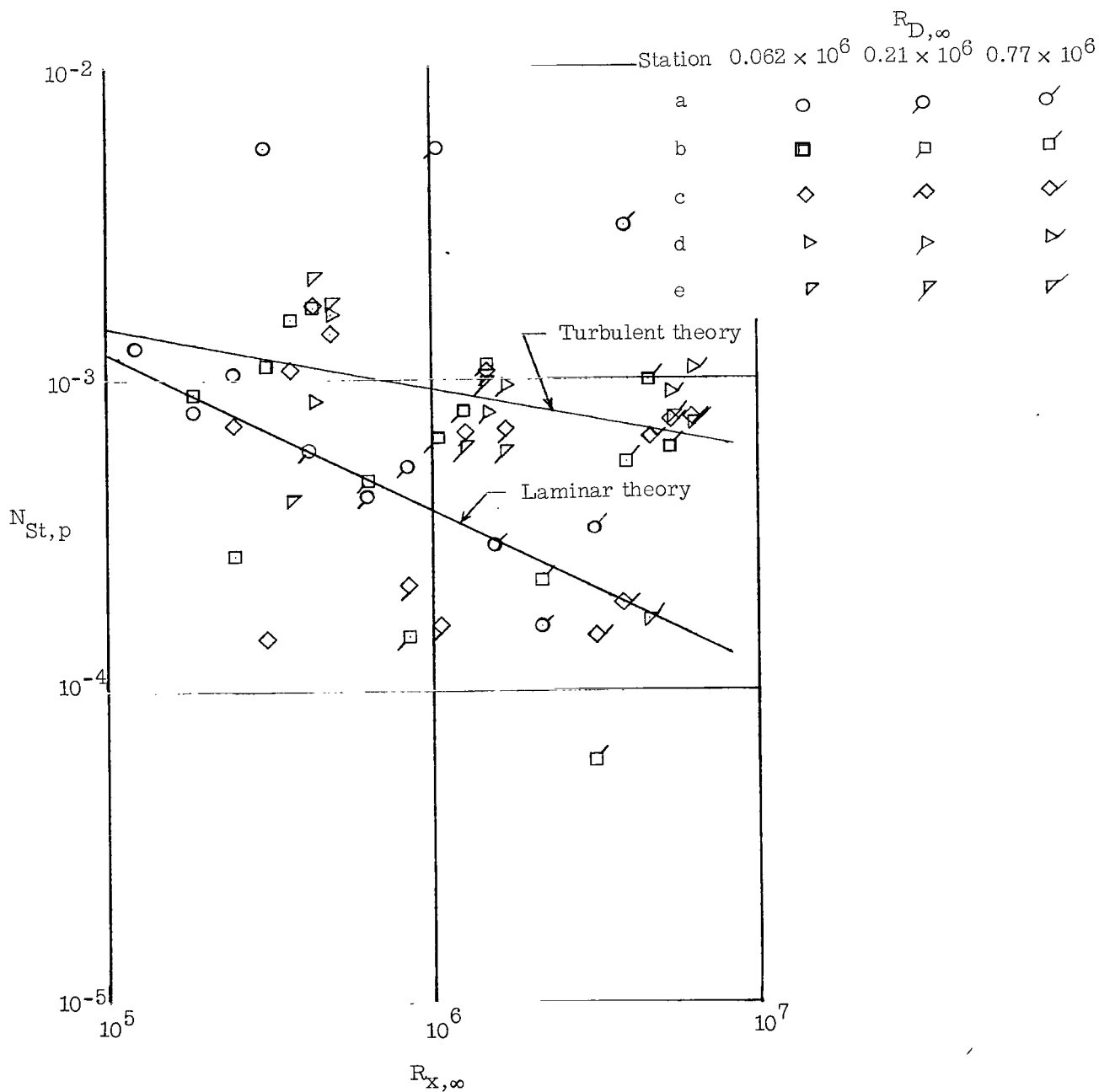

(b) $\beta = 30^{\circ}$.   L-64-431

Figure 12.- Schlieren photographs of shock impingement on plate. $\Lambda = 70^{\circ}$; $R_{D,\infty} \approx 0.2 \times 10^{6}$.

(a) $\beta = 0^\circ$.

Figure 13.- Variaton of heat-transfer distribution on plate with Reynolds number.

(b) $\beta = 25^{\circ}$.

Figure 13.- Concluded.

"The aeronautical and space activities of the United States shall be conducted so as to contribute . . . to the expansion of human knowledge of phenomena in the atmosphere and space. The Administration shall provide for the widest practicable and appropriate dissemination of information concerning its activities and the results thereof."

—NATIONAL AERONAUTICS AND SPACE ACT OF 1958

NASA SCIENTIFIC AND TECHNICAL PUBLICATIONS

TECHNICAL REPORTS: Scientific and technical information considered important, complete, and a lasting contribution to existing knowledge.

TECHNICAL NOTES: Information less broad in scope but nevertheless of importance as a contribution to existing knowledge.

TECHNICAL MEMORANDUMS: Information receiving limited distribution because of preliminary data, security classification, or other reasons.

CONTRACTOR REPORTS: Technical information generated in connection with a NASA contract or grant and released under NASA auspices.

TECHNICAL TRANSLATIONS: Information published in a foreign language considered to merit NASA distribution in English.

TECHNICAL REPRINTS: Information derived from NASA activities and initially published in the form of journal articles.

SPECIAL PUBLICATIONS: Information derived from or of value to NASA activities but not necessarily reporting the results of individual NASA-programmed scientific efforts. Publications include conference proceedings, monographs, data compilations, handbooks, sourcebooks, and special bibliographies.

Details on the availability of these publications may be obtained from:

SCIENTIFIC AND TECHNICAL INFORMATION DIVISION

NATIONAL AERONAUTICS AND SPACE ADMINISTRATION

Washington, D.C. 20546